Article

SOURCE DATA | TRANSPARENT PROCESS

THE EMBO JOURNAL

Surface dynamics of GluN2B-NMDA receptors controls plasticity of maturing glutamate synapses

Julien P Dupuis[1,2,‡], Laurent Ladépêche[1,2,‡], Henrik Seth[3], Lucie Bard[1,2,†], Juan Varela[1,2], Lenka Mikasova[1,2], Delphine Bouchet[1,2], Véronique Rogemond[4,5,6], Jérôme Honnorat[4,5,6], Eric Hanse[3] & Laurent Groc[1,2,*]

Abstract

NMDA-type glutamate receptors (NMDAR) are central actors in the plasticity of excitatory synapses. During adaptive processes, the number and composition of synaptic NMDAR can be rapidly modified, as in neonatal hippocampal synapses where a switch from predominant GluN2B- to GluN2A-containing receptors is observed after the induction of long-term potentiation (LTP). However, the cellular pathways by which surface NMDAR subtypes are dynamically regulated during activity-dependent synaptic adaptations remain poorly understood. Using a combination of high-resolution single nanoparticle imaging and electrophysiology, we show here that GluN2B-NMDAR are dynamically redistributed away from glutamate synapses through increased lateral diffusion during LTP in immature neurons. Strikingly, preventing this activity-dependent GluN2B-NMDAR surface redistribution through cross-linking, either with commercial or with autoimmune anti-NMDA antibodies from patient with neuropsychiatric symptoms, affects the dynamics and spine accumulation of CaMKII and impairs LTP. Interestingly, the same impairments are observed when expressing a mutant of GluN2B-NMDAR unable to bind CaMKII. We thus uncover a non-canonical mechanism by which GluN2B-NMDAR surface dynamics plays a critical role in the plasticity of maturing synapses through a direct interplay with CaMKII.

Keywords development; high-resolution imaging; lateral diffusion; long-term potentiation; synaptic plasticity

Subject Categories Membrane & Intracellular Transport; Neuroscience

DOI 10.1002/embj.201386356 | Received 22 July 2013 | Revised 23 December 2013 | Accepted 3 January 2014 | Published online 3 March 2014

EMBO J (2014) 33, 842–861

See also: **L Matt & JW Hell** (April 2014)

Introduction

Glutamatergic synapses mediate most of the excitatory neurotransmission in the brain, and changes in their strength have emerged as a cellular basis for learning and memory. These adaptive properties often require the activation of ionotropic glutamate NMDA receptors (NMDAR) and NMDAR-dependent calcium influx in the postsynaptic compartment. In addition to glutamate and co-agonists, activation of NMDAR requires membrane depolarization to remove the voltage-dependent magnesium block. The combined requirement for glutamate and postsynaptic depolarization enables NMDAR to detect coincident pre- and postsynaptic activity, a prerequisite for the induction of Hebbian synaptic plasticity such as long-term potentiation (LTP) (Collingridge *et al*, 2004). NMDAR are heterotetramers resulting from various combinations of GluN1, GluN2A-D, and GluN3 subunits, which confer specific biophysical and pharmacological properties to the receptors (Cull-Candy *et al*, 2001). As a consequence, the presence in synapses of either GluN2A- or GluN2B-containing NMDAR differentially influences synaptic plasticity (Yashiro & Philpot, 2008). In the hippocampus and cortex, the most abundant NMDAR subtypes are composed of GluN1 subunits associated with GluN2A and/or GluN2B subunits (Cull-Candy & Leszkiewicz, 2004). Within synapses, the ratio between GluN2A- and GluN2B-NMDAR is not uniform and varies between brain hemispheres, axonal inputs, and during brain development and synaptic refinements following sensory experience (Ito *et al*, 2000; Kawakami *et al*, 2003; Lau & Zukin, 2007; Yashiro & Philpot, 2008; Smith *et al*, 2009). Thus, depending on the physiological context, synapses adapt their GluN2-NMDAR signaling in order to appropriately modulate their integrative capacity.

In addition to these well-described adaptations in the GluN2A/2B-NMDAR synaptic ratio, rapid modifications have been reported to occur shortly after the induction of synaptic plasticity in hippocampal

1 Interdisciplinary Institute for Neuroscience, University de Bordeaux, UMR 5297, Bordeaux, France
2 CNRS, IINS UMR 5297, Bordeaux, France
3 Department of Physiology, Institute of Neuroscience and Physiology, The Sahlgrenska Academy, University of Goteborg, Goteborg, Sweden
4 Lyon Neuroscience Research Center, INSERM U1028/CNRS UMR 5292, Lyon, France
5 Hospices Civils de Lyon, Hôpital Neurologique, Bron, France
6 Université de Lyon, Université Claude Bernard Lyon 1, Lyon, France
*Corresponding author. Tel: +33557575746; Fax: +33557574080; E-mail: laurent.groc@u-bordeaux2.fr
‡These authors equally contributed to this work.
†Present address: University College London, London, UK

neurons from neonatal rats (Bellone & Nicoll, 2007; Matta *et al*, 2011). While these fast changes could be one of the keys of synaptic metaplasticity, the cellular pathways and the adaptive role of this rapid GluN2A/2B switch remain unknown. Here, we addressed these issues using a combination of single nanoparticle tracking and electrophysiology in hippocampal neurons. Within the plasma membrane, NMDAR laterally diffuse in a GluN2 subunit-dependent manner and thereby explore large areas around synapses (Tovar & Westbrook, 2002; Groc *et al*, 2004, 2006; Bard *et al*, 2010). We report that following LTP induction, the synaptic distribution of surface GluN2B-NMDAR—but not GluN2A-NMDAR—rapidly changes through an increase in surface diffusion. Strikingly, this lateral rearrangement appears to be instrumental for LTP expression. Indeed, anti-GluN1/2B subunit antibodies, originating either from immunized animals or from encephalitis patients with memory deficits and neuropsychiatric symptoms, acutely abolish NMDAR surface diffusion and consequently prevent LTP at hippocampal synapses. While the activity-dependent upregulation of GluN2B-NMDAR surface diffusion is regulated by calcium-calmodulin-activated kinase CaMKII and casein kinase II (CKII) activity, we show that it also requires the direct binding of CaMKII to GluN2B. Thus, through a direct interaction, GluN2B-NMDAR surface dynamics control the activity-dependent recruitment of CaMKII to spines during LTP induction in developing hippocampal networks.

Results

Synaptic GluN2B-NMDAR lateral diffusion is rapidly increased during $_{chem}$LTP in immature neurons

Although NMDAR were long thought to be rather static within synapses, the discovery of their surface dynamics and fast signaling changes during synaptic plasticity opened the possibility that these receptors might undergo rapid remodeling during synaptic adaptation processes. Initially, the surface diffusion of NMDAR was characterized in cultured hippocampal neurons using single nanoparticle tracking, fluorescent recovery after photobleaching (FRAP) imaging, and electrophysiologial approaches (Tovar & Westbrook, 2002; Groc *et al*, 2006, 2007a; Michaluk *et al*, 2009; Bard *et al*, 2010). It was also recently shown in hippocampal brain slices that pre-synaptic NMDAR laterally diffuse in the membrane (Yang *et al*, 2008), but whether postsynaptic surface receptors are also mobile in slice still remained a matter of debate (Harris & Pettit, 2007). To directly address this challenging issue, we expressed in hippocampal neurons the GluN2B subunit fused to a Super Ecliptic pHluorin (SEP) at its extracellular N-terminus (GluN2B-SEP) to isolate surface GluN2B-NMDAR (Supplementary Methods). SEP is a pH-sensitive variant of GFP that only emits fluorescence at neutral pH; fluorescence is quenched at acidic pH, such as in intracellular vesicles (Ashby *et al*, 2006). We expressed GluN2B-SEP in pyramidal neurons from organotypic hippocampal slices through gene-gun transfection (see Materials and Methods), then imaged brain slices using the FRAP approach to directly measure the surface diffusion of GluN2B-NMDAR in apical dendrites of CA1 pyramidal neurons (Supplementary Fig S1), and compared the corresponding mobile fraction values with those obtained from cultured hippocampal neurons. After photobleaching, a significant fraction of GluN2B-SEP fluorescence recovered in slices (~35%) (Supplementary Fig S1). In cultured dissociated hippocampal neurons expressing GluN2B-SEP after chemical transfection (see Materials and Methods), approximately 30% of GluN2B-SEP fluorescence recovered after 160 s (Supplementary Fig S1). Together, these FRAP imaging data unequivocally demonstrate that surface GluN2B-NMDAR diffuse similarly in cultured neurons and intact hippocampal preparations.

As mentioned above, glutamatergic synapses might regulate their NMDAR content and surface dynamics in an activity-dependent manner. Pioneer electrophysiological experiments in brain slices from neonatal rodents have demonstrated that shortly after LTP induction, the synaptic GluN2A/2B-NMDAR ratio rapidly changes (Bellone & Nicoll, 2007), suggesting that a fast trafficking of GluN2-NMDAR is tightly coupled to the synaptic activity status. Both activities of NMDAR and mGluR5 receptors are required for this synaptic activity-dependent GluN2B/2A switch and play a critical role in the experience-dependent regulation of NMDAR subunit composition (Matta *et al*, 2011). To identify the cellular mechanisms involved in these processes, we used single-particle (quantum dot, "QD") tracking in cultured hippocampal neurons to image the local surface dynamics of GluN2A- and GluN2B-NMDAR subtypes within synaptic areas during LTP (Dahan *et al*, 2003; Groc *et al*, 2004, 2007b). A bath application of glycine and picrotoxin was used to promote the synaptic insertion of AMPA glutamate receptors (AMPAR), referred herein as chemical LTP "$_{chem}$LTP" (Lu *et al*, 2001, 2007; Wang *et al*, 2008), a protocol that was shown to induce an NMDAR-dependent increase in the synaptic content in GluA1-AMPAR and consequently the amplitude of AMPAR-mediated miniature EPSCs (Groc *et al*, 2008; Petrini *et al*, 2009). Consistently, $_{chem}$LTP increased (~20% on average) the fluorescence intensity associated with SEP-GluA1-AMPAR inside synapses detected using Homer 1c-DsRed fluorescence (Fig 1A and B). QD-GluN2A- and QD-GluN2B-NMDAR were then tracked over time within Homer 1c-DsRed-labeled postsynaptic densities before and immediately after $_{chem}$LTP induction. Under basal conditions, synaptic GluN2A-NMDAR were less mobile and more enriched in synapses than GluN2B-NMDAR (Fig 1C), as previously described (Groc *et al*, 2006, 2007a; Bard *et al*, 2010). Strikingly, GluN2B-NMDAR surface mobility was significantly increased 1-4 min following $_{chem}$LTP induction in the synaptic area, which includes the postsynaptic density and perisynaptic area (320-nm annulus) (Fig 1D and E). This effect was (i) specific for GluN2B-NMDAR since GluN2A-NMDAR surface diffusion remained unaffected (Fig 1D and E), (ii) mostly attributable to a reduced fraction of immobile receptors (membrane diffusion < 0.005 $\mu m^2/s$), and (iii) prevented by a bath application of the NMDAR antagonist AP5 (50 μM) (Fig 1E). Tens of minutes after $_{chem}$LTP induction, the diffusion of the remaining synaptic GluN2B-NMDAR was close to basal value (0.03 ± 0.015 $\mu m^2/s$, $n = 10$ neurons, $P > 0.05$ compared to control value), indicating that the upregulation of GluN2B-NMDAR diffusion is transient. Collectively, these data show that the induction of $_{chem}$LTP is associated with a rapid increase in lateral diffusion of synaptic GluN2B-NMDAR in a NMDAR-dependent fashion. We then tested whether this effect persisted independently of the maturation stage by comparing $_{chem}$LTP-induced changes in GluN2B-NMDAR lateral diffusion in immature (7–12 div) and mature (14–21 div) neurons. Interestingly, mature neurons did not display $_{chem}$LTP-induced upregulation in the lateral diffusion of GluN2B-NMDAR (Fig 1F), although synapses still underwent a

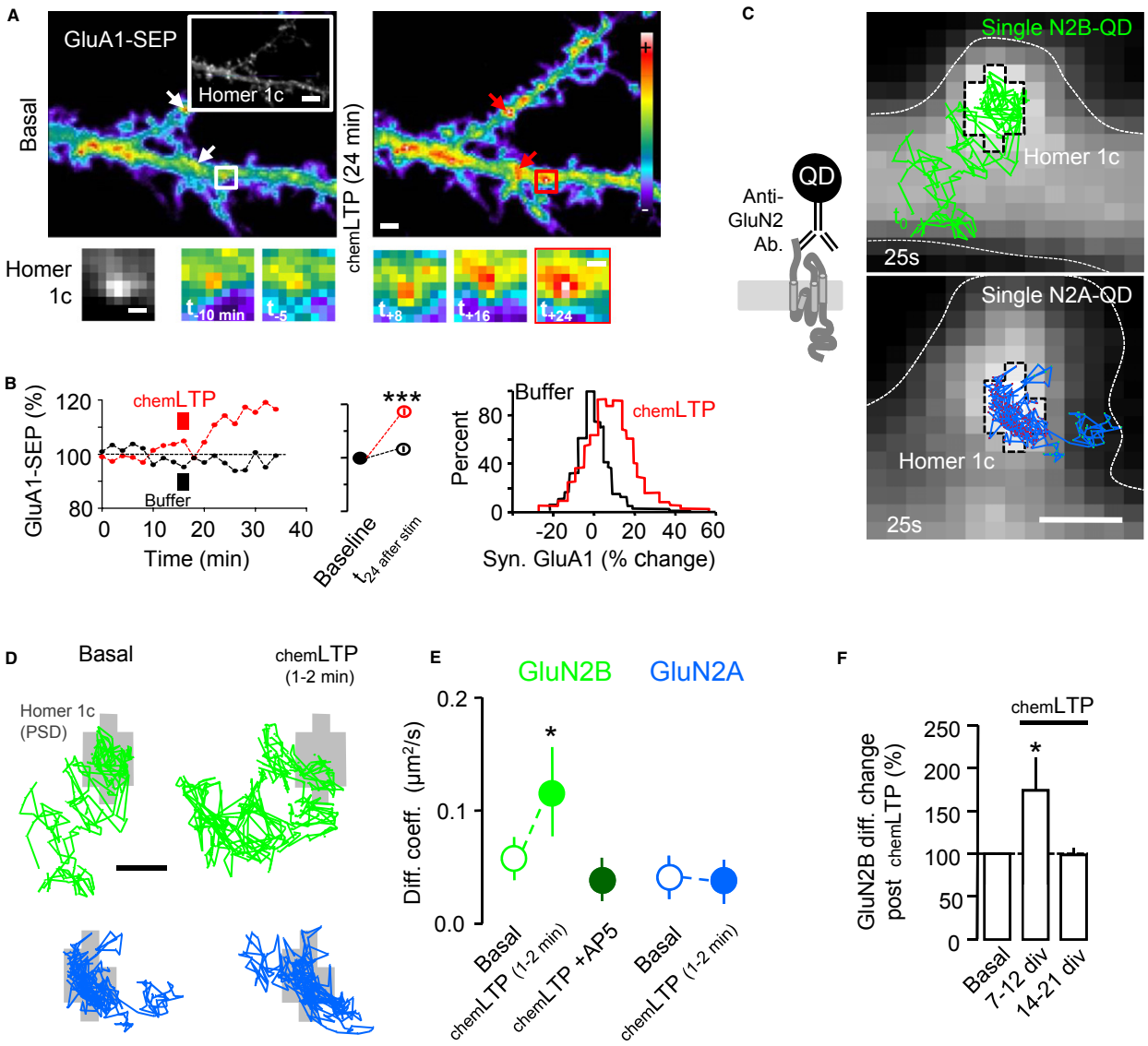

Figure 1. The surface diffusion of synaptic GluN2B-NMDAR is rapidly increased after $_{chem}$LTP in immature neurons.

A Upper panels: Representative dendritic fragments of a hippocampal neuron (13 div) expressing GluA1-SEP and Homer 1c-DsRed. Clusters of GluA1-SEP were imaged for at least 30 min. The pseudocolor representation shows the different intensity levels of the GluA1-SEP staining. GluA1-SEP intensity was measured in synapses (Homer1c cluster) before and after the induction of $_{chem}$LTP (see Materials and Methods). Note that 10 min after $_{chem}$LTP, the GluA1-SEP fluorescence intensity increased in postsynaptic clusters. Arrows designate synapses (i.e., Homer). Bottom panels: magnifications and time-lapses of the outlined GluA1-SEP synaptic clusters. Scale bar = 5 μm; insets = 500 nm; bottom panels = 350 nm.

B Left panel: Representative example of a GluA1-SEP fluorescence time course before and after $_{chem}$LTP (red) or buffer (black) protocol. The average GluA1-SEP synaptic intensity was significantly increased after $_{chem}$LTP (24 min after induction) (middle panel). Student's *t*-test, ***$P < 0.001$. Right panel: distribution of the change in synaptic GluA1-SEP content under control (black line, $n = 364$ syn. clusters) and $_{chem}$LTP (red line, $n = 837$) conditions. Note the right shift in the distribution, indicating an increased proportion of synaptic GluA1-AMPAR after $_{chem}$LTP.

C Left: Schematic drawing of a single QD–antibody complex targeting a surface NMDAR. Right: Representative trajectories (25-s duration, 30-Hz acquisition) of surface QD-conjugated GluN2B- (top, green line) and GluN2A-NMDAR (bottom, blue line) in Homer 1c-GFP-labeled synaptic areas (black dotted line) in an immature hippocampal neuron (11 div). Scale bar = 5 μm.

D Representative GluN2A- and GluN2B-NMDAR trajectories during baseline and right after $_{chem}$LTP (1–4 min). Note the lateral displacement of synaptic GluN2B-NMDAR after $_{chem}$LTP. The postsynaptic densities are represented by the gray shapes. Scale bar = 0.75 μm.

E Comparison of the instantaneous membrane diffusion coefficients of synaptic GluN2A- and GluN2B-NMDAR in different experimental conditions. Note that GluN2B-NMDAR membrane diffusion coefficients are significantly increased right after $_{chem}$LTP (1–2 min; $n = 15$, *$P < 0.05$). This increase is prevented by a bath application of a competitive NMDAR antagonist, AP5 (50 μM, $n = 6$, Mann-Whitney test, $P > 0.05$). GluN2A-NMDAR membrane diffusion coefficients are not significantly changed by $_{chem}$LTP ($n = 19$, $P > 0.05$). The symbols represent the mean ± s.e.m.

F Comparison of the $_{chem}$LTP-elicited change in synaptic GluN2B-NMDAR surface diffusion (median normalized to baseline for each condition) in immature (7–12 div) and mature (14–21 div) neurons. Bar graphs represent mean ± s.e.m. Mann-Whitney test, *$P < 0.05$.

significant increase in synaptic GluA1-AMPAR content (+11 ± 1%, of GluA1-SEP in live neurons; $P < 0.05$) arguing in favor of a developmentally regulated process.

Synaptic GluN2B-NMDAR are laterally displaced from the postsynaptic density during $_{chem}$LTP

Activity-dependent changes in GluN2B-NMDAR surface dynamics might affect the receptor distribution in the synaptic area. Taking advantage of the accuracy of single nanoparticle detection properties (Fig 2A) (Groc *et al*, 2007b; Triller & Choquet, 2008), we therefore investigated the surface distribution of GluN2A- and GluN2B-NMDAR before and during $_{chem}$LTP induction. On the representative synaptic areas shown in Fig 2B, a 500-frame stack was used to elaborate a map of the successive locations of either a GluN2A- or a GluN2B-NMDAR. The synaptic area was arbitrarily divided into two zones: the PSD and the perisynaptic area (320-nm annulus surrounding PSD). Consistent with electron microscopy observations

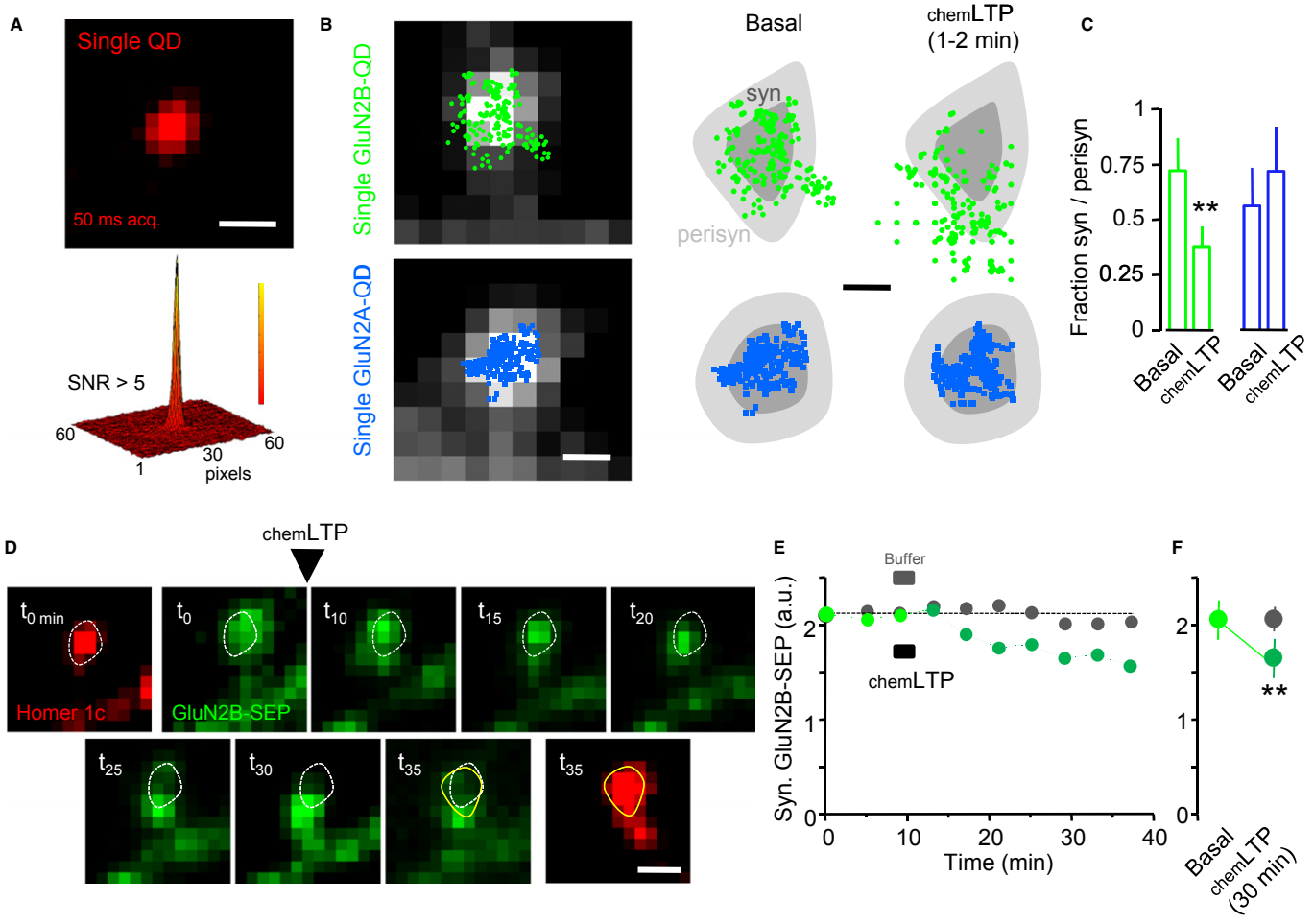

Figure 2. Synaptic GluN2B-NMDAR are laterally redistributed in the synaptic area following $_{chem}$LTP in immature neurons.

A Detection of a single QD (30-Hz acquisition) in our experimental conditions. The high signal-to-noise ratio (SNR) (> 5) enables the detection and location of the signal with a high pointing accuracy (~30 nm). The QD fluorescence is quantified on a pseudocolor scale (low: red; high: yellow). Scale bar = 800 nm.

B A 500-frame stack is obtained while tracking down a single NMDAR/QD complex. On each frame, a single GluN2B- (green) or GluN2A- (blue) QD particle complex is detected and precisely located within synaptic (dark gray) and perisynaptic (320-nm annulus around the synapse; light gray) areas. Those 500 locations are then projected on a single image, providing the successive positions of this receptor/particle complex during the 500-frame stack. Note that GluN2A-NMDAR are more concentrated within the core of the PSD. Scale bar image = 300 nm; synaptic areas = 200 nm.

C Relative fraction of synaptic and perisynaptic GluN2-QD particles, calculated before and after $_{chem}$LTP for both GluN2B- (left) and GluN2A-NMDAR (right) (n = 25 and 20 dendritic fields before and after $_{chem}$LTP, respectively). Note the significant decrease in the relative synaptic content in GluN2B-NMDAR particles right after $_{chem}$LTP (Student's t-test, $^{**}P < 0.01$).

D Time-lapse imaging of GluN2B-SEP in an immature hippocampal neuron (10 div) before and after $_{chem}$LTP. The GluN2B-SEP fluorescence was followed in glutamate postsynaptic area (Homer 1c-DsRed; white dotted line). Homer 1c fluorescence was imaged at the beginning and at the end of the recording (35 min). Note that the Homer 1c fluorescence intensity and area increased 35 min after $_{chem}$LTP (yellow full line). Scale bar = 800 nm.

E Representative time-lapse recording of GluN2B-SEP fluorescence within synapses (Homer 1c area) before and after buffer (gray dots) and $_{chem}$LTP (green dots) application.

F Average GluN2B-SEP fluorescence before (basal) and 30 min after buffer (gray dot; n = 14; paired test, $P > 0.05$) or $_{chem}$LTP (green dot; n = 23; paired Student's t-test, $^{**}P < 0.01$).

Data information: Error bars in bar graphs represent mean ± s.e.m.

Figure 3. Surface cross-linking of NMDAR specifically impairs their surface diffusion without affecting their function.

A Trajectories of single surface QD-GluN1-NMDAR (30-Hz acquisition, 30-s duration) in hippocampal neurons in control (left) and GluN1x-link (right) conditions. A schematic representation of the NMDAR x-link technique using primary anti-GluN (I^{ary} Ab) and secondary (II^{ary} Ab) antibodies is shown in the middle panel. Insets: enlarged GluN1-QD trajectories. Field scale bar = 5 μm; inset scale bar = 1 μm.

B Cumulative distribution of GluN1-NMDAR instantaneous surface diffusion coefficients in control and GluN1x-link conditions. Note the leftward shift of the curve in the GluN1x-link condition, indicating a slowdown of surface diffusion.

C Representative FRAP acquisition of GluA1-SEP in control and GluN1-NMDAR x-link conditions. The circles indicate the bleached regions. Scale bar = 5 μm.

D Average FRAP recovery curves of GluA1-SEP fluorescence in control (n = 13), GluN1 x-link (n = 3), and GluN2B x-link (n = 4) conditions. Full lines represent the average recovery, while dotted lines represent the mean ± s.e.m. The fluorescence recovery of surface synaptic GluA1-SEP remained unaffected in all conditions ($P > 0.05$).

E Representative images of a hippocampal neuron in the basal condition or after glutamate (30 μM) application. The pseudocolor representation shows the different intensity levels of the calcium indicator (Fluo4-AM, 2 μM) before and after the glutamate stimulation. Scale bar = 20 μm.

F Average calcium intensity change (ΔF/F0) over time after glutamate stimulation of hippocampal neurons (n = 29).

G Relative comparison (percent of basal) of a transient calcium rise induced by glutamate in control (n = 29), control + AP5 (n = 12, Student's t-test, $^{**}P < 0.01$ when compared to control), and GluN1-NMDAR x-link (n = 21).

H Representative recordings of spontaneous NMDAR-mediated EPSC in control (black trace) or GluN1 x-link (gray trace) condition. Averaged sEPSC are shown below. Note the perfect overlay of the averaged NMDAR sEPSC in both conditions.

I Comparisons of NMDAR sEPSC inter-event interval, amplitude, decay, and rise times (control, n = 8; GluN1 x-link, n = 9; Student's t-test, $P > 0.05$ for all parameters).

Data information: Data in (F), (G) and (I) are presented as mean ± s.e.m.

(Shinohara *et al*, 2008), it could be noted that under basal conditions, GluN2A-NMDAR were more concentrated in the PSD area than GluN2B-NMDAR. Following $_{chem}$LTP induction, synaptic GluN2B-NMDAR were rapidly displaced toward peri- and extrasynaptic areas, whereas GluN2A-NMDAR remained stable (Fig 2B and C), leading to an increased GluN2A/2B-NMDAR synaptic ratio. These single nanoparticle detection data thus provide direct evidence that during synaptic potentiation the distribution of GluN2B-NMDAR is rapidly and locally modified. We finally confirmed these data by imaging over time the content of surface GluN2B-SEP in glutamate synapses (Fig 2D). Two to four minutes after $_{chem}$LTP induction, a decrease in GluN2B-SEP fluorescence intensity was observed within the synaptic area (Fig 2D and E), reaching a plateau approximately 10 min after $_{chem}$LTP induction and remaining stable over 30 min (Fig 2E). On average, $_{chem}$LTP induction produced a small (15%) but significant decrease in GluN2B-SEP staining in the PSD (Fig 2E and F). Altogether, these data indicate that the induction of $_{chem}$LTP is associated with a lateral reorganization of GluN2B-NMDAR in the synaptic/perisynaptic area, raising the possibility that this surface redistribution could play a role in the adaptation of glutamate synapses in immature neurons.

An antibody directed against NMDAR specifically impairs receptor surface diffusion without affecting its function

The fact that $_{chem}$LTP induction is paralleled by a lateral redistribution of GluN2B-NMDAR does not necessarily imply that the two are causally related. To directly test whether the lateral dynamics of surface GluN2B-NMDAR is involved in the establishment of $_{chem}$LTP, we first implemented an *in vitro* approach to artificially immobilize surface NMDAR. To achieve this, we used a previously described cross-linking (x-link) protocol (Groc *et al*, 2008; Heine *et al*, 2008), in which primary antibodies directed against extracellular epitopes of GluN subunits and then secondary antibodies directed against the primary antibodies were successively incubated with cultured hippocampal neurons (Fig 3A). We first quantified the effect of GluN1 x-link on GluN1-NMDAR surface diffusion using single QD-GluN1 tracking. Applying a GluN1 x-link (20 min) onto hippocampal neurons significantly reduced the surface diffusion of GluN1-NMDAR, as attested by a leftward shift in the cumulative distributions of GluN1-NMDAR diffusion coefficients (Fig 3A and B) and a significant increase in the fraction of immobile GluN1-NMDAR from 52 to 75% in the presence of GluN1 x-link (Fig 3B). Because a single QD can potentially interact with several antibodies, we used a complementary approach to ascertain the impact the x-link procedure on receptor surface diffusion which consisted in performing fluorescent recovery after photobleaching (FRAP) experiments in hippocampal neurons transfected with GluN1-SEP. Applying anti-GluN1 subunit and secondary antibodies significantly increased the fraction of immobile surface GluN1-NMDAR (from 36 to 50%) (Supplementary Fig S2). To note, performing an anti-GluN2B subunit x-link had a similar impact on surface diffusion of GluN1-NMDAR (Supplementary Fig S2). Since a fraction of the GluN1-SEP subunits recovered in these conditions, we also tested the impact of an anti-GFP x-link protocol that targets with a very high efficacy surface GluN1/2B-SEP. Consistent with the endogenous receptor data, this protocol immobilized approximately 60% of GluN1-SEP (Supplementary Fig S2). Importantly, neither the anti-GluN1 nor anti-GluN2B subunit x-link changed the GluA1-SEP (AMPAR) surface FRAP (Fig 3C–D), indicating that both the GluN1 and GluN2B x-link protocols specifically impair the surface diffusion of NMDAR without affecting AMPAR.

We next investigated the impact of the GluN1 x-link protocol on the synaptic NMDAR content and function. To this end, we first tested whether GluN1 x-link (30–60 min) altered the GluN1-NMDAR synaptic content by measuring the fluorescence of synaptic GluN1-SEP clusters (co-localizing with Homer 1c) in the absence or presence of extracellular anti-GluN1 antibodies. The GluN1-NMDAR content in Homer 1c clusters was not significantly altered after GluN1 x-link (Supplementary Fig S3), indicating that the reduction in GluN1-NMDAR surface dynamics does not alter the synaptic pool of NMDAR. We have previously shown that a x-link of GluA1-AMPAR does not affect the amplitude, kinetics, and single channel conductance of AMPAR synaptic currents (Heine *et al*, 2008). Similarly, to ascertain that NMDAR channel function was not impaired by the GluN1 x-link procedure, we first monitored NMDAR-dependent calcium changes in hippocampal neurons by briefly applying glutamate (30 μM) in the presence of a cocktail of AMPAR, mGluR, Na^+ channel, and L-type Ca^{2+} channel antagonists (Fig 3E and F). The calcium rise observed in these conditions was fully blocked in the presence of AP5, confirming its NMDAR dependency (Fig 3G).

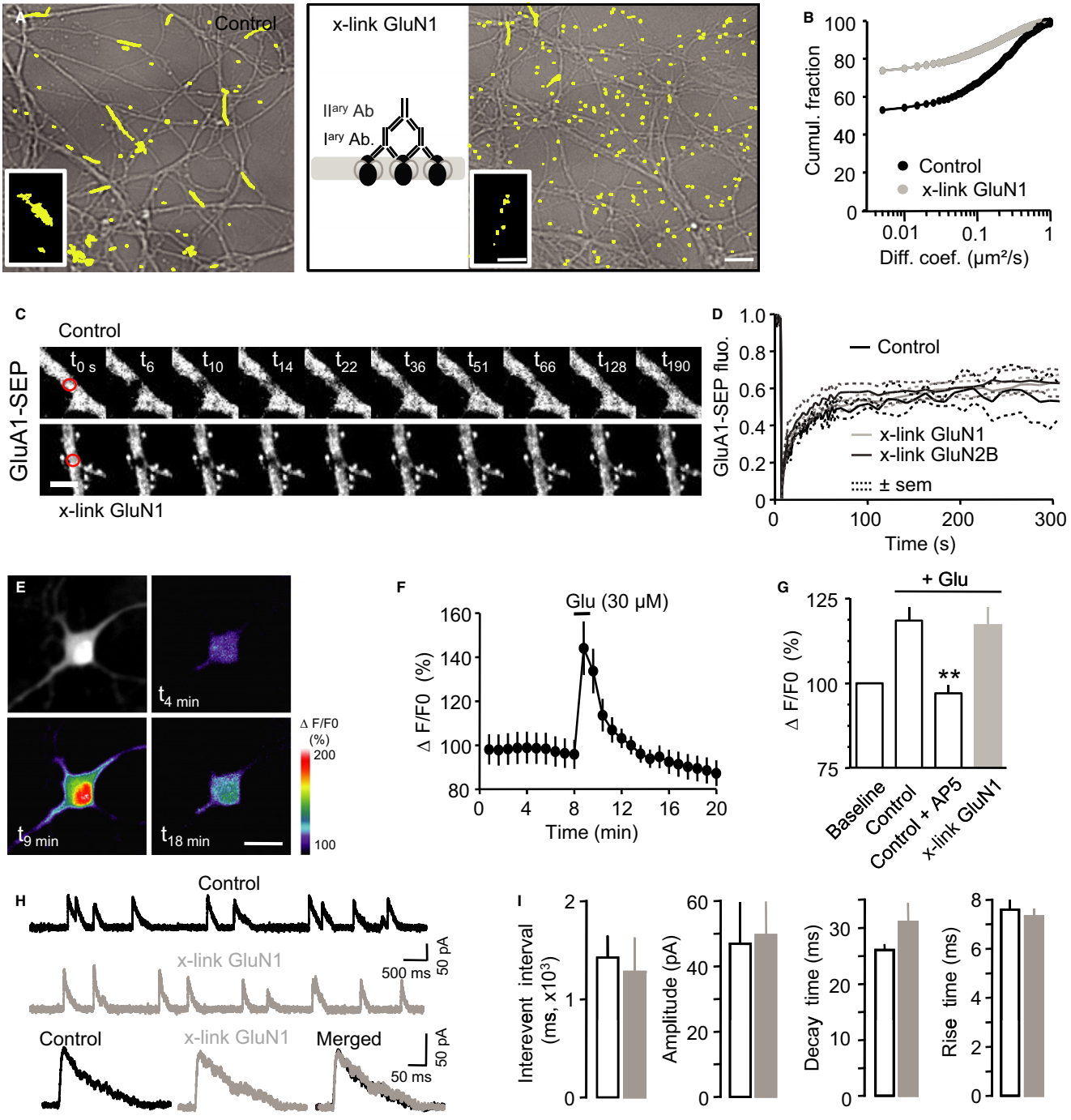

Notably, the NMDAR-mediated calcium rise was not affected by the presence of GluN1 x-link (Fig 3G), indicating that the binding of extracellular antibodies to surface NMDAR subunits does not affect the calcium-permeant properties of NMDAR. Finally, we recorded spontaneous NMDAR-mediated EPSCs from neurons exposed to GluN1 x-link (30–60 min) and compared the sEPSC inter-event interval, amplitude, and kinetics with control conditions. Neither of these parameters was altered by GluN1 x-link, confirming that the NMDAR-mediated currents and synaptic content were not modified by the GluN1x-link procedure (Fig 3H and I). Altogether, these data demonstrate that the surface dynamics of NMDAR can be artificially, efficiently, and specifically reduced using antibodies directed against extracellular epitopes and that this x-link protocol does not alter receptor activity, synaptic content, or basal transmission within this time period.

NMDAR surface dynamics is required to enable $_{chem}$LTP in hippocampal cultured neurons

Whether the $_{chem}$LTP-associated changes in GluN2B-NMDAR surface diffusion and distribution are consequential or causal to $_{chem}$LTP induction is an important question. To directly address this

point, we measured the relative content of GluA1-SEP (AMPAR) in Homer 1c clusters during $_{chem}$LTP induction in the presence or absence of GluN x-link. As reported above, synaptic GluA1-SEP fluorescence was stable over time (Fig 1A) and GluN1 x-link alone did not alter the synaptic content in GluA1-AMPAR (Fig 4A). Strikingly, reducing GluN1-NMDAR surface diffusion by GluN1 x-link completely prevented the $_{chem}$LTP induction, affecting both the expected increase in the synaptic content in GluA1-SEP-AMPAR and the number of "potentiated" synapses (those in which the GluA1 subunit content is increased by ≥ 2 s.d. above the average basal receptor content) (Fig 4B–D). Since $_{chem}$LTP induced a specific change in GluN2B-NMDAR lateral distribution, we then specifically immobilized surface GluN2B-NMDAR using a GluN2B x-link protocol. This procedure prevented $_{chem}$LTP induction as efficiently as the GluN1-NMDAR x-link (Fig 4B–D). Because these data were obtained in neuronal preparations containing a low level of glial cells, which could possibly bias synaptic adaptation processes (Henneberger *et al*, 2010), we then confirmed the effect of GluN x-link on $_{chem}$LTP in hippocampal cultures containing astroglia (Supplementary Fig S4). Finally, GluN1- and GluN2B-NMDAR x-link protocols also blocked $_{chem}$LTP-induced increase in the synaptic content of endogenous GluA2-AMPAR as measured by immunocytochemistry (Fig 4E and F). A prediction from the imaging data is that preventing GluN2A-NMDAR surface diffusion should not alter the AMPAR $_{chem}$LTP since GluN2A-NMDAR dynamics was not altered by activity. Consistently, GluN2A-NMDAR x-link protocol did not prevent the potentiation of glutamate synapses after $_{chem}$LTP ($24 \pm 4\%$ of potentiated synapses after $_{chem}$LTP, $n = 9$, $P < 0.001$). Finally, we tested whether another LTP protocol is sensitive to GluN x-link. We used a forskolin/rolipram cocktail that promotes an increase in intracellular cAMP levels through the activation of adenylyl cyclase and the inhibition of cAMP phosphodiesterase activity, part of the early phase being independent of NMDAR (Lu & Gean, 1999; Otmakhov *et al*, 2004a,b). The forskolin/rolipram protocol rapidly potentiated GluA1-AMPAR in glutamate synapses, and this process was not prevented by the application of GluN1-NMDAR x-link (Fig 4G). Thus, glycine-induced LTP is sensitive to NMDAR cross-linking, while a forskolin-induced one is not.

Altogether, these data demonstrate that reducing specifically GluN1/2B-NMDAR surface dynamics blocks NMDAR-dependent AMPAR $_{chem}$LTP in hippocampal glutamate synapses.

Ex vivo and *in vivo* acute blockade of NMDAR surface dynamics prevents LTP in CA3-CA1 hippocampal synapses

Although we demonstrated that reducing GluN1-NMDAR surface dynamics prevents $_{chem}$LTP-induced NMDAR-dependent AMPAR potentiation *in vitro*, the question remained whether similar mechanisms would also participate in NMDAR-dependent LTP induction in *ex vivo* brain preparations. To address this point, we first recorded fEPSP evoked by stimulation of the Schaffer collaterals in the CA1 area of acute hippocampal slices from young animals (P15–20). In control conditions, five trains of 20 impulses at 100 Hz induced a robust LTP visible as an increase in the slope of the fEPSP (Fig 5B–D). Interestingly, acute incubation of the slices with anti-GluN1 subunit antibody x-link preparation (Fig 5A) reduced by half the magnitude of LTP (Fig 5C and D). Indeed, the mean fEPSP slope 20–25 min after the LTP-inducing trains was increased when compared to the baseline ($157 \pm 13.5\%$, $n = 8$), whereas it was significantly lower following 45 min of incubation in rabbit polyclonal antibodies directed against GluN1 ($120 \pm 6\%$, $n = 8$). To note, GluN1-NMDAR x-link by itself did not alter the fEPSP magnitude over time (Fig 5C and D). Since we observed a developmental down-regulation of the activity-dependent increase in GluN2B-NMDAR lateral dynamics, we performed the same experiment in older hippocampal preparations (P31–45). Consistent with the imaging data, GluN1-NMDAR x-link produced a weaker effect in adult preparations, that is, a non-significant reduction in the magnitude of LTP (Fig 5D). Thus, these data indicate that GluN1-NMDAR x-link strongly impairs LTP in acute hippocampal slices, an effect more pronounced in immature hippocampal networks.

Since anti-GluN1 subunit antibodies may not fully penetrate and invade acute slices by bath incubation, we then performed *in vivo* hippocampal stereotaxic injections of either a buffer, control goat anti-rabbit IgG, or GluN1 x-link (Fig 5E; see Materials and Methods) in young rats (P10–15), and recorded evoked AMPAR-mediated EPSC in CA1 pyramidal neurons from acute hippocampal slices prepared 1 h after injection. To note, the injection procedures did not alter the overall amplitude of AMPAR-mediated EPSC (control: 114 ± 6 pA, $n = 6$; control IgG: 123 ± 6 pA, $n = 7$; GluN1 x-link: 118 ± 8 pA, $n = 7$; $P > 0.05$), indicating that the presence of IgG (control and anti-NMDAR) does not modify basal synaptic transmission and that GluN1 x-link *per se* does not affect the content of functional synaptic AMPAR. We then used a pairing protocol to elicit NMDAR-dependent LTP at CA3-CA1 synapses in the three different paradigms. In control condition, pairing induced a persistent increase in EPSC amplitude (Fig 5F–H), which was prevented by a bath application of the NMDAR antagonist AP5 (50 μM; not shown). However, consistently with the imaging data, GluN1 x-link fully prevented LTP expression (Fig 5F–H). To note, injecting goat anti-rabbit IgG did not affect LTP expression (Fig 5F–H), nor did injecting anti-NMDAR IgG in the vicinity of the hippocampus (i.e., entorhinal cortex; not shown). Altogether, these electrophysiological data demonstrate that GluN1 x-link prevents LTP in the CA1 hippocampal circuitry *ex vivo*, strengthening the non-canonical and primary role of fast NMDAR surface reorganization during NMDAR-dependent synaptic plasticity processes.

Anti-NMDAR autoantibodies from patients with cognitive deficits acutely prevent synaptic potentiation without affecting NMDAR function

While the GluN1/2B x-link experiments clearly support a role for NMDAR surface dynamics in synaptic plasticity, the physiological relevance of an artificial x-link of surface receptors had to be addressed. Interestingly, autoimmune synaptic encephalitis is a recently described human brain disease leading to neuropsychiatric syndromes through inappropriate brain–autoantibodies interactions (Moscato *et al*, 2010; Vincent *et al*, 2010). The most frequent form of synaptic autoimmune encephalitis is associated with autoantibodies directed against extracellular epitopes of the GluN1-NMDAR, with patients first suffering from short-term memory deficits and later from neuropsychiatric symptoms (Dalmau *et al*, 2007, 2008; Chapman & Vause, 2011). Immunotherapy leads to rapid recovery, indicating that the interplay between NMDAR autoantibodies and network functions is reversible (Lee *et al*, 2009; Dalmau *et al*,

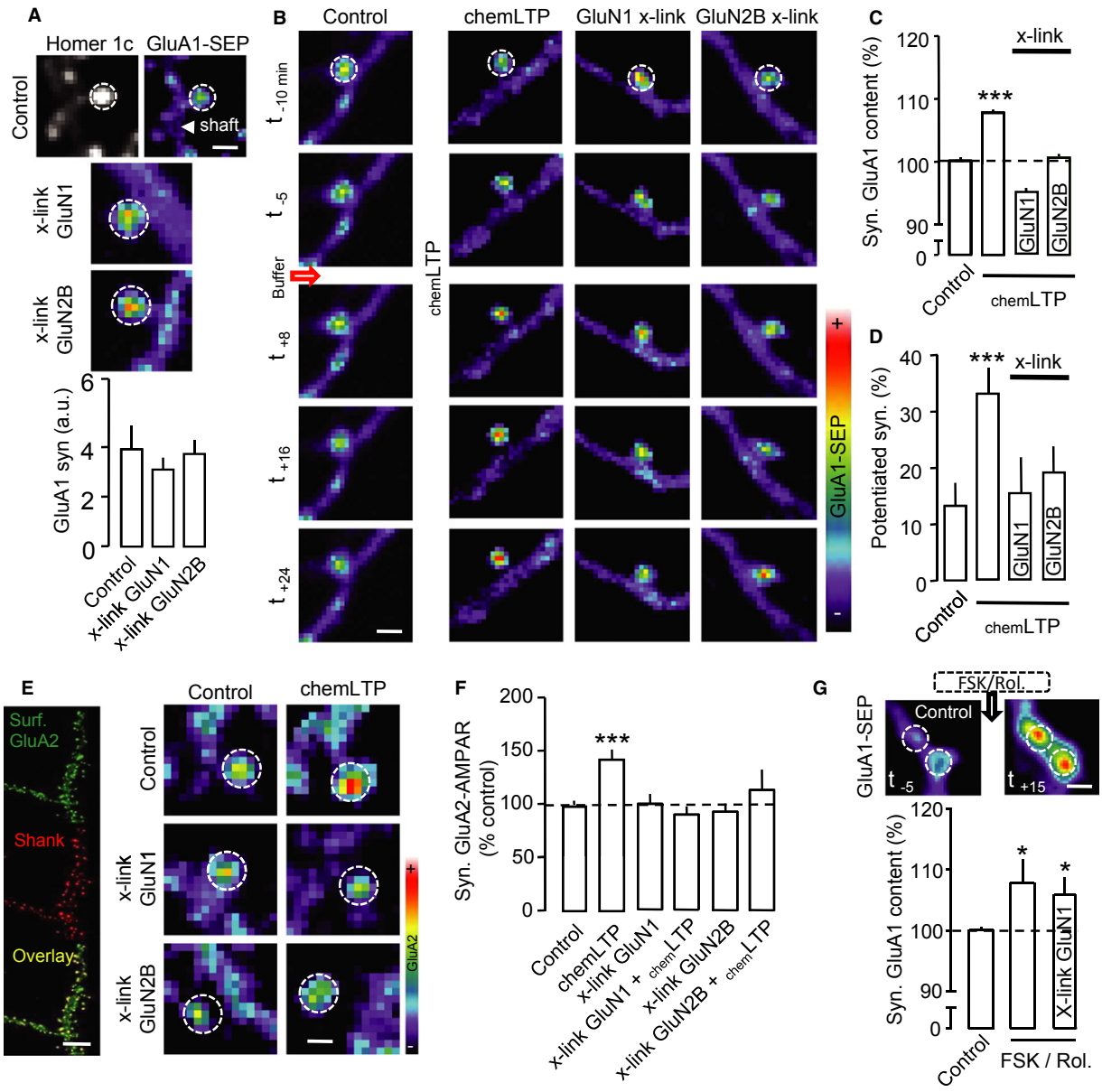

Figure 4. The surface cross-linking of NMDAR blocks $_{chem}$LTP.

A Comparison of the GluA1-SEP fluorescence within synapses (white dotted circle) in spines from control (n = 786 synapses), GluN1 x-link (n = 1324), or GluN2B x-link (n = 987) condition. The dendritic shaft is indicated by the arrow head. Scale bar = 1 μm. The bar graphs represent the mean value ± s.e.m.

B Time-lapse imaging of spine areas containing GluA1-SEP (white dotted circle) from immature hippocampal neurons in control (no stimulation), $_{chem}$LTP, $_{chem}$LTP + GluN1 x-link, and $_{chem}$LTP + GluN2B x-link conditions. The pseudocolor representation shows the different intensity levels of the GluA1-SEP staining. Scale bar = 1 μm.

C Comparison of the normalized GluA1-SEP fluorescence intensity within synapses in control (n = 786 synapses), $_{chem}$LTP alone (n = 1324, ***P < 0.001 when compared to control), $_{chem}$LTP + GluN1 x-link (n = 736, P > 0.05), and $_{chem}$LTP + GluN2B x-link (n = 966, P > 0.05) conditions. ANOVA followed by Newman-Keuls Multiple Comparison Test.

D Comparison of the percentage of potentiated synapses in control (n = 364), $_{chem}$LTP alone (n = 837, ***P < 0.001), $_{chem}$LTP + GluN1 x-link (n = 312, P > 0.05), and $_{chem}$LTP + GluN2B x-link (n = 472 syn. clusters, P > 0.05) conditions. ANOVA followed by Newman-Keuls Multiple Comparison Test.

E Representative image of surface GluA2-AMPAR (green) and postsynaptic density protein Shank (red) immunostaining. Scale bar = 5 μm. Right panel, GluA2-SEP fluorescence was detected in spines in control, GluN1 x-link, and GluN2B x-link, before and after $_{chem}$LTP. Scale bar = 500 nm.

F Quantification of GluA2-AMPAR content in synapses. As for GluA1-AMPAR, $_{chem}$LTP (n = 98 dendritic fields) increased GluA2-AMPAR synaptic content. This was blocked in GluN1- (n = 24 dendritic fields) and GluN2B-NMDAR (n = 6 dendritic fields) x-link conditions when compared to their respective control conditions (n = 113, n = 19 and n = 12 dendritic fields, respectively). ANOVA followed by Newman-Keuls Multiple Comparison Test, ***P < 0.001.

G Bar graph: Comparison of the GluA1-SEP fluorescence content within synapses in control (n = 370 synapses), forskolin/rolipram (FSK/Rol.; n = 550 synapses; *P < 0.05), and FSK/Rol. + GluN1 x-link (n = 558 synapses; *P < 0.05) conditions. ANOVA followed by Newman-Keuls Multiple Comparison Test. Data are presented as mean ± s.e.m. Top panels: representative images showing increased GluA1-SEP fluorescence within synapses (white dotted circles) after forskolin/rolipram application. Scale bar = 2.5 μm.

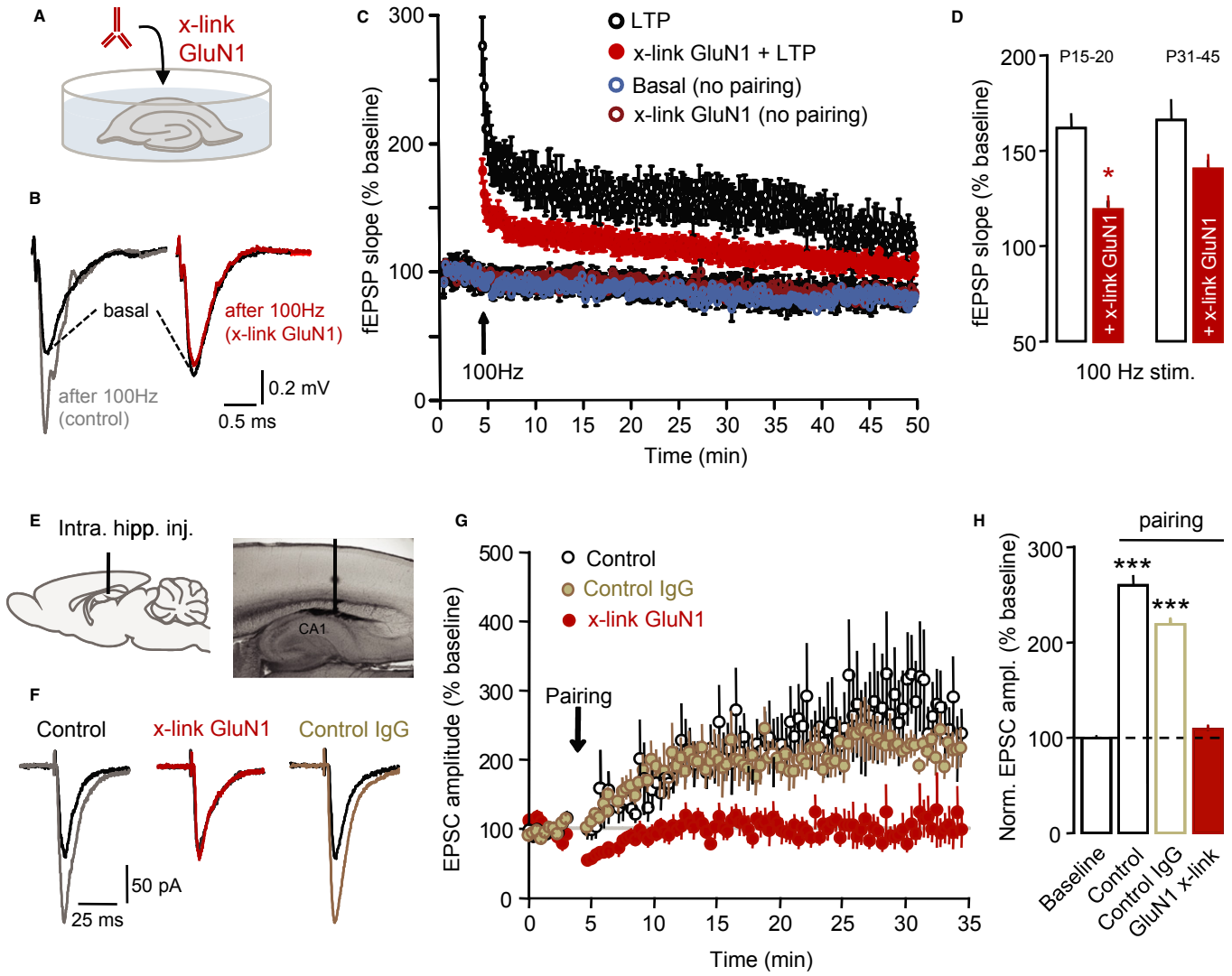

Figure 5. Acute GluN1-NMDAR x-link prevents LTP at CA3-CA1 synapse in rat hippocampal slices.

A–C Slices from P15 to 20 Wistar rats were incubated in a regular (control) or anti-GluN1-supplemented ACSF (x-link GluN1) for 45 min prior to fEPSP recordings (A). Average field responses in various conditions are represented (B). A robust LTP, as measured by the slope of the fEPSP, was induced by five trains of 20 pulses at 100 Hz (C). LTP amplitude decreased over the first 5 min before reaching a stable plateau. Cross-linking the GluN1 subunits with antibody substantially decreased LTP amplitude. There was no difference in fEPSP slope between control (n = 8) and x-link GluN1 (n = 8) under basal condition ($P > 0.05$). Recordings without LTP-inducing trains either in GluN1 x-link or in control ASCF did not change over time.

D Mean normalized fEPSP slope after 100-Hz stimulation in control (n = 8; open bar) and GluN1 x-link (n = 8; red bar) conditions from P15 to 20 (Student's t-test, $^*P < 0.05$ between control and GluN1 x-link conditions) and P31–45 rats.

E Schematic description of the stereotaxic injection of rabbit anti-GluN1 polyclonal antibodies or goat anti-rabbit IgG (0.4 μg/μl) into the dorsal hippocampus. Right panel: representative example of a rat hippocampal slice showing the antibody injection site labeled with black ink.

F GluN1 x-link prevented NMDAR-dependent pairing-induced LTP at CA3-CA1 synapses from P10 to 15 rats. Representative EPSC traces recorded during the baseline (gray) or 25–30 min after the induction protocol in control condition (black) or following stereotaxic injection of rabbit polyclonal antibodies directed against GluN1 (X-link, red) or goat anti-rabbit IgG (control IgG, light brown).

G Average time course of the pairing-induced LTP. Normalized EPSC amplitudes (normalization to the mean amplitude of EPSCs recorded during baseline acquisition) are plotted against time for control (black, n = 6), x-link (red, n = 7), and control IgG (light brown, n = 7) conditions. Data are presented as mean ± s.e.m.

H Mean of normalized EPSC amplitudes at baseline or 25–30 min after application of the pairing protocol in control condition (black; 260 ± 9.7%, n = 6), or following stereotaxic injection of rabbit polyclonal antibodies directed against GluN1 (x-link, red; 109.1 ± 3.8%, n = 7) or goat anti-rabbit IgG (control IgG, light brown; 218.9 ± 4.6%, n = 7). GluN1 x-link prevented NMDAR-dependent LTP expression (control versus x-link, $P < 0.0001$; control IgG versus x-link, $^{***}P < 0.0001$). ANOVA followed by Newman-Keuls Multiple Comparison Test. Bars represent mean ± s.e.m.

2011). The autoantibodies recognize an identified extracellular epitope of the GluN1 subunit leading to massive GluN1/2-NMDAR surface content changes (Dalmau *et al*, 2008; Hughes *et al*, 2010; Gleichman *et al*, 2012; Mikasova *et al*, 2012). Here, we purified IgG against NMDAR from cerebrospinal fluid of encephalitis patients (Fig 6A) (Manto *et al*, 2007) and tested their acute impact on

$_{chem}$LTP induction. As it has been previously and thoroughly demonstrated (Dalmau *et al*, 2008; Hughes *et al*, 2010; Gleichman *et al*, 2012; Mikasova *et al*, 2012), we here simply confirmed that patients' IgG recognize GluN1 subunits in hippocampal neurons (Fig 6A), prevent NMDAR surface diffusion as assessed by GluN2B-NMDAR diffusion (Fig 6B), and do not affect NMDAR channel function by showing that glutamate-induced NMDAR-mediated calcium bursts were not affected in the presence of IgG (Fig 6C). We then incubated neurons with purified patient or control IgG for 20–25 min, induced $_{chem}$LTP, and monitored changes in GluA1-AMPAR synaptic content over time. In the control IgG condition, the synaptic content in GluA1-AMPAR (comparison between neurons, Fig 6D; comparison between clusters, +11 ± 3% after $_{chem}$LTP, n = 96 clusters, $P < 0.01$) and the number of potentiated synapses increased after $_{chem}$LTP, consistent with our previous results (Fig 4). It could be noted that we here compared GluA1 cluster. However, patient IgG directed against NMDAR acutely prevented $_{chem}$LTP expression as the synaptic content in GluA1-AMPAR and the percentage of potentiated synapses remained unchanged (Fig 6D), as early as 10 min after autoantibody incubation. Consistent with this result, patient IgG were similarly reported to acutely (5- to 10-min exposure) block theta burst-induced LTP at CA3-CA1 synapses

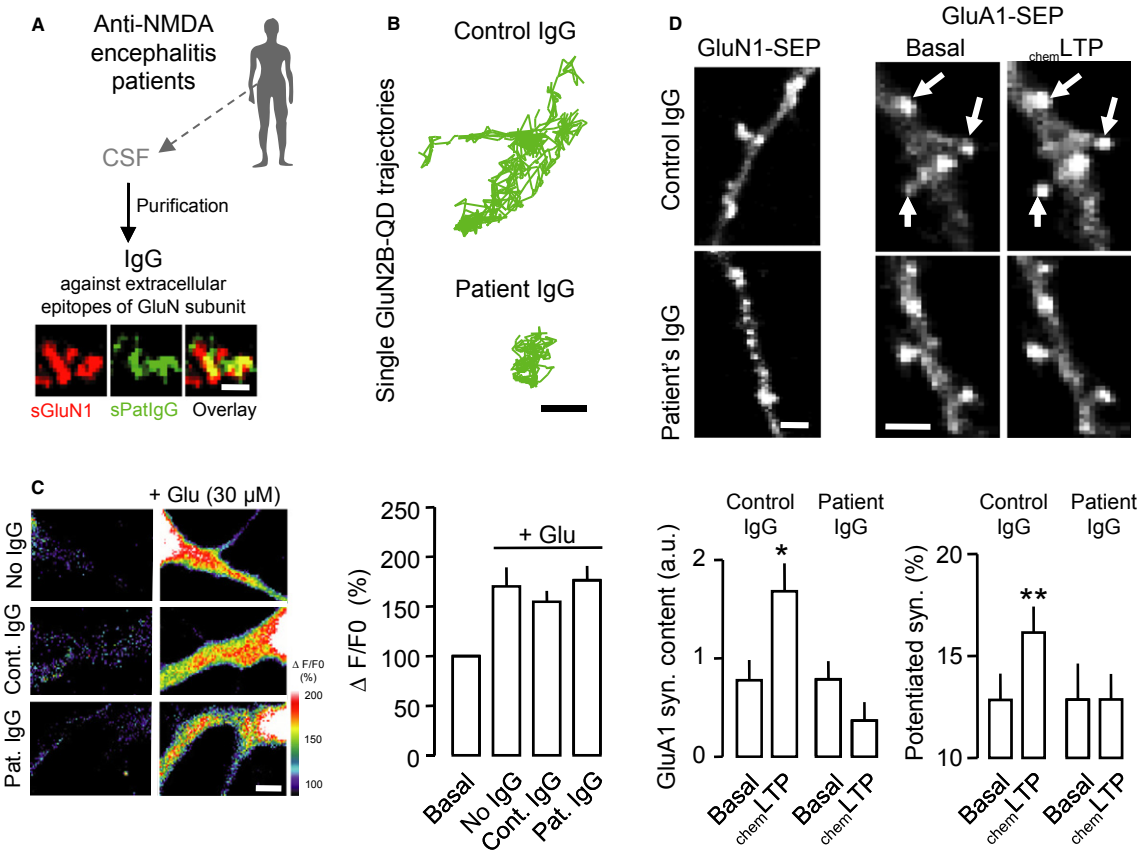

Figure 6. Antibodies against extracellular epitopes of NMDAR from autoimmune encephalitis patients acutely prevent $_{chem}$LTP.

A Schematic diagram of the anti-NMDAR IgG isolation procedure from anti-NMDAR encephalitis patients. The cerebrospinal fluid (CSF) was collected and IgG were purified for *in vitro* imaging experiments. Lower panels: note the high co-localization of surface staining from surface patient anti-NMDAR IgG ("sPat. IgG," green) and commercial anti-GluN1 antibodies (sGluN1, red). Scale bar = 1 µm.

B Representative GluN2B-NMDAR-QD trajectories from neurons incubated either with control or with patient IgG. Note the massive reduction in surface dynamics. Scale bar = 250 nm.

C Representative images of hippocampal neurons in the basal conditions or after glutamate (30 µM) application. The pseudocolor representation shows the different intensity levels of the calcium indicator (Fluo4-AM, 2 µM) before and after the glutamate stimulation. Neurons were incubated either with no IgG, controls IgG (Cont. IgG), or patients IgG (Pat. IgG). Scale bar = 20 µm. Right panel: Average calcium intensity change (ΔF/F0) over time after glutamate stimulation of hippocampal neurons in no IgG, controls IgG (Cont. IgG), or patients IgG (Pat. IgG) conditions.

D Hippocampal neurons expressing either GluN1-SEP or GluA1-SEP were incubated with IgG (5 µg/ml) either from control or from anti-NMDAR patients for 20–25 min. Note that patient IgG do not affect GluN1-SEP distribution. Neurons were stimulated with a $_{chem}$LTP protocol and each synaptic GluA1-AMPAR cluster was followed over time. Note that $_{chem}$LTP increased the intensity of GluA1-SEP in synaptic clusters (arrows) only in control IgG condition. Scale bars = 1 µm. Lower panels: Quantification of the GluA1-AMPAR synaptic content and percentage of potentiated GluA1-AMPAR synapses in control or patient IgG conditions. For each neuron, GluA1 synaptic fluorescence intensity was quantified before and 10–15 min after $_{chem}$LTP. The GluA1-AMPAR synaptic content and percentage of potentiated GluA1-AMPAR synapses significantly increased in control condition (n = 6 neurons; Student's t-test, *$P < 0.05$ for GluA1 synaptic content, **$P < 0.01$ for the percentage of potentiated GluA1 synapses) but not in the presence of patient IgG (n = 9, $P > 0.05$ in all parameters). ANOVA followed by Newman-Keuls Multiple Comparison Test. Bars represent mean ± s.e.m.

(Zhang *et al*, 2012). Together, these results show that anti-NMDAR autoantibodies, which induce memory deficits and neuropsychiatric symptoms in a titer-dependent manner in patients, acutely prevent LTP induction.

The activity-dependent alteration of GluN2B-NMDAR surface dynamics is regulated by CaMKII activity and direct binding to GluN2B subunit

Intracellular signaling molecules, such as protein kinases, are strongly implicated in the trafficking of NMDAR and induction of NMDAR-dependent forms of LTP (Chen & Roche, 2007). To assess their potential involvement in the $_{chem}$LTP-elicited increase in lateral diffusion of GluN2B-NMDAR, we tracked receptors before and during $_{chem}$LTP in the presence of either the Ca^{2+}/calmodulin-dependent protein kinase II (CaMKII) inhibitors KN93 (20 μM), AIP2 (5 μM), KN62 (5 μM), the protein kinase A inhibitor KT 5720 (10 μM), the protein kinase C inhibitor Gö 6976 (10 μM), or the casein kinase 2 (CKII) inhibitors TMCB (10 μM) and TBB (10 μM). While the $_{chem}$LTP-induced increase in GluN2B-NMDAR mobility was not affected by KT 5720 or Gö 6976, it was fully blocked by the application of KN93, AIP2, KN62, TBB, or TMCB (Fig 7A and B). It could be noted that a short pre-incubation with TBB (10 min, 10 μM) was not sufficient to prevent the effect (not shown), and only pre-exposure longer than 4 h was effective (Sanz-Clemente *et al*, 2010). Thus, among the protein kinases listed above, CaMKII and CKII activities, which are required for GluN2B-NMDAR synaptic trafficking and LTP induction (Lisman *et al*, 2002; Sanz-Clemente *et al*, 2010), appear to be involved in the activity-dependent upregulation of GluN2B-NMDAR lateral diffusion. Of interest, activation of the metabotropic glutamate receptor 5 (mGluR5) has been reported to be required for the activity-dependent GluN2B/2A switch (Matta *et al*, 2011). We tracked GluN2B-NMDAR before and during $_{chem}$LTP induction in the presence of MPEP (10 μM) or MTEP (10 μM), two selective non-competitive antagonists of mGluR5. Blocking mGluR5 activity during $_{chem}$LTP prevented the increase in lateral diffusion of GluN2B-NMDAR (MPEP, $n = 1{,}200$ trajectories, $P > 0.05$; MTEP, $n = 5{,}777$ trajectories, $P > 0.05$), further supporting a role of mGluR5 in this process.

When we examined the impact of CaMKII and CKII activities on GluN2B-NMDAR surface diffusion, it appeared that CaMKII is deeply involved in the regulation of the basal dynamics of both extrasynaptic and synaptic GluN2B-NMDAR, whereas CKII seems to play a limited role (Fig 7A and C). A further exploration of the behavior of surface GluN2B- and GluN2A-NMDAR using a single molecule approach (Groc *et al*, 2007b; Groc & Choquet, 2008) confirmed that CaMKII inhibition strongly reduces the dynamics of synaptic GluN2B-NMDAR, while it has no effect on synaptic GluN2A-NMDAR (Supplementary Fig S5). In addition to phosphorylation, CaMKII has been shown to directly interact with the C-terminal tail of the GluN2B subunit, and this interaction regulates the intracellular trafficking of GluN2B-NMDAR (Barria & Malinow, 2005). To evaluate whether this direct interaction could also impact the surface diffusion of GluN2B-NMDAR, we took advantage of a dual point mutation (R1300Q/S1303D) in GluN2B, which blocks the binding of CaMKII (Strack *et al*, 2000). When compared to wild-type, GluN2B-RQ/SD surface diffusion in the synaptic compartment was significantly reduced (Fig 7C), suggesting a prominent role of the GluN2B/CaMKII interaction in the regulation of GluN2B-NMDAR dynamics within synaptic areas. One could thus speculate that this interaction might play a role in the activity-dependent regulation of GluN2B-NMDAR in synapses. To address this point, neurons were transfected with either wild-type GluN2B-SEP or GluN2B-RQ/SD and these receptors were tracked within synaptic areas before and after $_{chem}$LTP. Strikingly, the absence of direct interaction between GluN2B-NMDAR and CaMKII prevented the activity-dependent upregulation of GluN2B-NMDAR surface dynamics (Fig 7D and E), indicating that besides phosphorylation, CaMKII directly contributes to the fast lateral redistribution of GluN2B-NMDAR during LTP through their physical interaction.

GluN2B-NMDAR surface dynamics directly impact on CaMKII trafficking to spines

How could a reduced NMDAR surface diffusion prevent LTP induction without altering the receptor synaptic content or biophysical function? We demonstrated above that the activity-dependent lateral redistribution of GluN2B-NMDAR depends on the activation and direct interaction with CaMKII, which by itself is critical for the induction of LTP. Once activated by calcium entry through NMDAR, CaMKII is translocated to spines and becomes enriched in the PSD (Shen & Meyer, 1999; Bayer *et al*, 2001; Otmakhov *et al*, 2004b), where it is stabilized over time (Sharma *et al*, 2006). Interestingly, the direct interaction between CaMKII and GluN2B plays a prominent role in LTP and memory functions (Bayer *et al*, 2006; Sanhueza *et al*, 2011; Halt *et al*, 2012; Lisman *et al*, 2012). Based on these studies and our data, one may expect that through their direct interaction, the upregulated surface dynamics of GluN2B-NMDAR might directly contribute to the reorganization of CaMKII during LTP. To address this question, we took advantage of the x-link protocol to specifically alter NMDAR surface dynamics while imaging CaMKII trafficking. We first tested whether the x-link procedure by itself affected the GluN2B/CaMKII interaction using a co-immunoprecipitation assay. We report that GluN1 x-link does not alter the interaction between GluN2B and CaMKII (α form), as well as with the phosphorylated CaMKII-Thr286 form (Fig 8A). We also tested the impact of GluN1 x-link on CaMKII basal content and reported no significant change in CaMKII enrichment in spines (basal: 2.3 ± 0.2 a.u., $n = 7$; x-link GluN1: 2.4 ± 0.2 a.u., $n = 7$; $P > 0.05$). We then assessed the impact of GluN1 x-link on the evolution of CaMKII content in spines before and after $_{chem}$LTP. Consistent with the literature, $_{chem}$LTP increased the CaMKII content in spines (10–15 min after induction) (Fig 8B). Surprisingly, GluN1x-link prevented this increase and it even produced a significant reduction in the spine CaMKII content (Fig 8B), indicating that NMDAR surface diffusion influences the CaMKII content in spines and suggesting a functional link between the NMDAR surface dynamics and CaMKII redistribution. To further address this point, we investigated whether NMDAR x-link affects the intracellular trafficking of CaMKII before and after $_{chem}$LTP induction. The intracellular dynamics of CaMKII-GFP was imaged in dendritic spines using the FRAP approach (Fig 8C–D, Supplementary Fig S6). Shortly after $_{chem}$LTP induction (5–15 min), the mobile fraction of CaMKII-GFP increased significantly to 126% of its basal value (Fig 8D, Supplementary Fig S6A), consistent with an increased flux of CaMKII to spines. However, when $_{chem}$LTP was applied to neurons exposed to GluN1x-link, the mobile fraction of

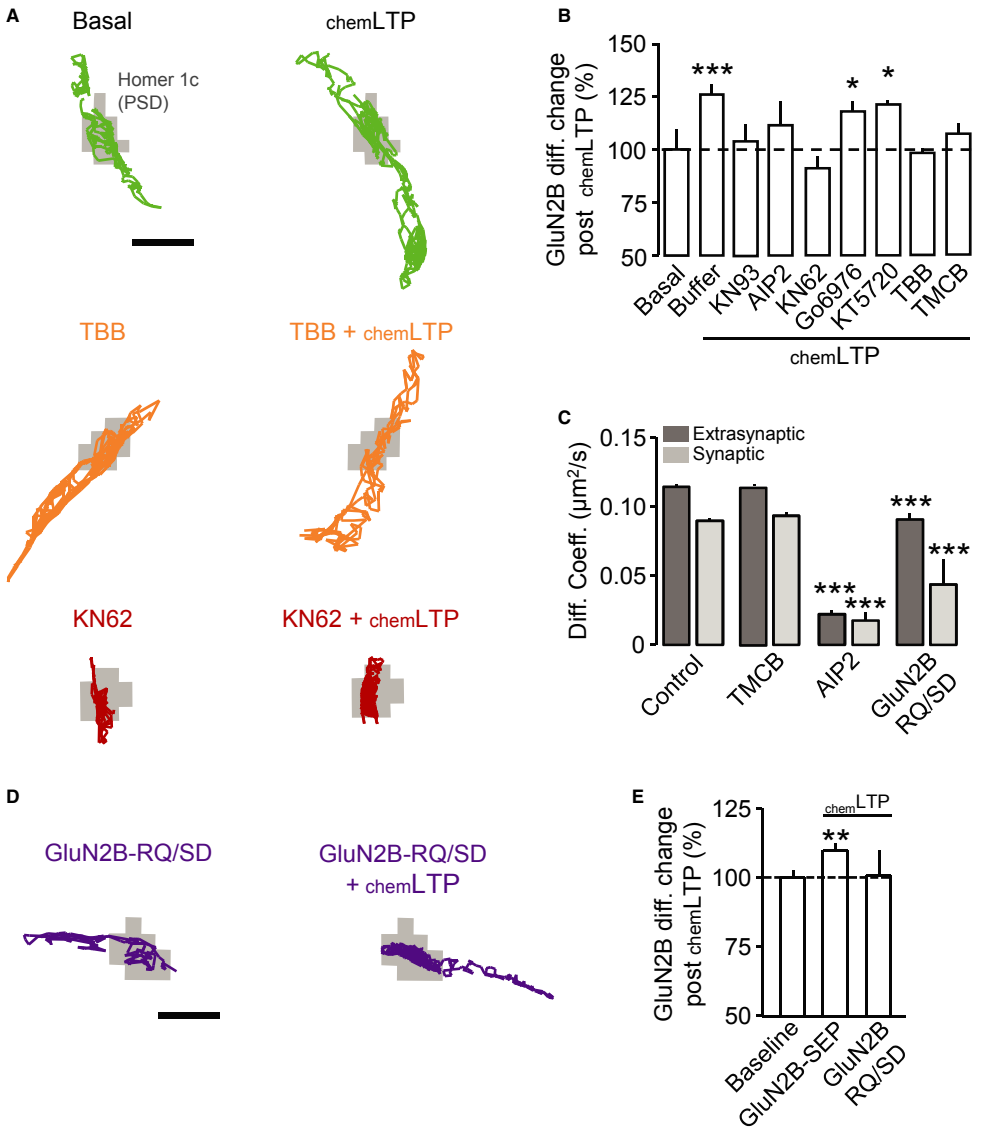

Figure 7. Regulation of GluN2B-NMDAR surface dynamics by CAMKII and CKII activities.

A Representative trajectories (25-s duration, 20-Hz acquisition) of surface QD-conjugated GluN2B-NMDAR within Homer 1c-GFP-labeled synaptic areas (gray) before and after $_{chem}$LTP in immature hippocampal neuron (9–12 div) in control (green), TBB (orange), and KN62 (red) conditions. Scale bar = 1 μm.

B Synaptic GluN2B-NMDAR surface diffusion change (normalized to baseline for each condition) after $_{chem}$LTP in immature neurons (< 12 div) pre-incubated (15 min) with either buffer (PBS, n = 3,388 trajectories, ***P < 0.001), CaMKII inhibitors KN93 (5 μM, n = 1,521, P > 0.05), AIP2 (5 μM, n = 1,199, P > 0.05), or KN62 (5 μM, n = 3,088, P > 0.05), PKC inhibitor Gö6976 (10 μM, n = 3,175, *P < 0.05), PKA inhibitor KT5720 (10 μM, n = 847, *P < 0.05), and CK2 inhibitors TBB (10 μM, 4 h pre-incubation, n = 3,322, P > 0.05) or TMCB (10 μM, n = 1,200, P > 0.05). Kruskal-Wallis followed by Dunns Multiple Comparison Test, for all P-values.

C Mean extrasynaptic and synaptic GluN2B-NMDAR diffusion coefficients in control condition (extrasynaptic, n = 6,160 trajectories; synaptic, n = 4,199 trajectories), in the presence of the CK2 inhibitor TMCB (10 μM; extrasynaptic, n = 7,889 trajectories; synaptic, n = 2,427 trajectories; Mann-Whitney test, P > 0.05 compared to control) or the CaMKII inhibitor AIP2 (5 μM; extrasynaptic, n = 772 trajectories; synaptic, n = 86 trajectories; Mann-Whitney test, ***P < 0.0001 compared to control), and mean extrasynaptic and synaptic GluN2B-(R1300Q/S1303D)-NMDAR diffusion coefficients (GluN2B-RQ/SD; extrasynaptic, n = 880 trajectories; synaptic, n = 29 trajectories; Mann-Whitney test, ***P < 0.0001 compared to control).

D Representative trajectories (25-s duration, 20-Hz acquisition) of surface QD-conjugated GluN2B-(R1300Q/S1303D)-NMDAR(GluN2B-RQ/SD) within Homer 1c-GFP-labeled synaptic areas (gray) before and after $_{chem}$LTP in immature hippocampal neuron (9–12 div). Scale bar = 1 μm.

E Synaptic GluN2B-SEP and GluN2B-RQ/SD surface diffusion change (normalized to baseline for each condition) after $_{chem}$LTP (GluN2B-SEP, n = 1,498 trajectories, baseline versus $_{chem}$LTP, Student's t-test, **P < 0.01; GluN2B-RQ/SD, n = 323 trajectories, baseline versus $_{chem}$LTP, Mann-Whitney test, P < 0.05).

Data information: In (B), (C) and (E), data are presented as mean ± s.e.m.

CaMKII-GFP remained unaltered (Fig 8D, Supplementary Fig S6A). Remarkably, the same was observed in non-treated neurons expressing GluN2B-RQ/SD (Fig 8D), indicating that the direct interaction between GluN2B and CaMKII plays a key role in the spine trafficking of CaMKII during the onset of plasticity. Because the trafficking of other intracellular interactors of NMDAR could also potentially be

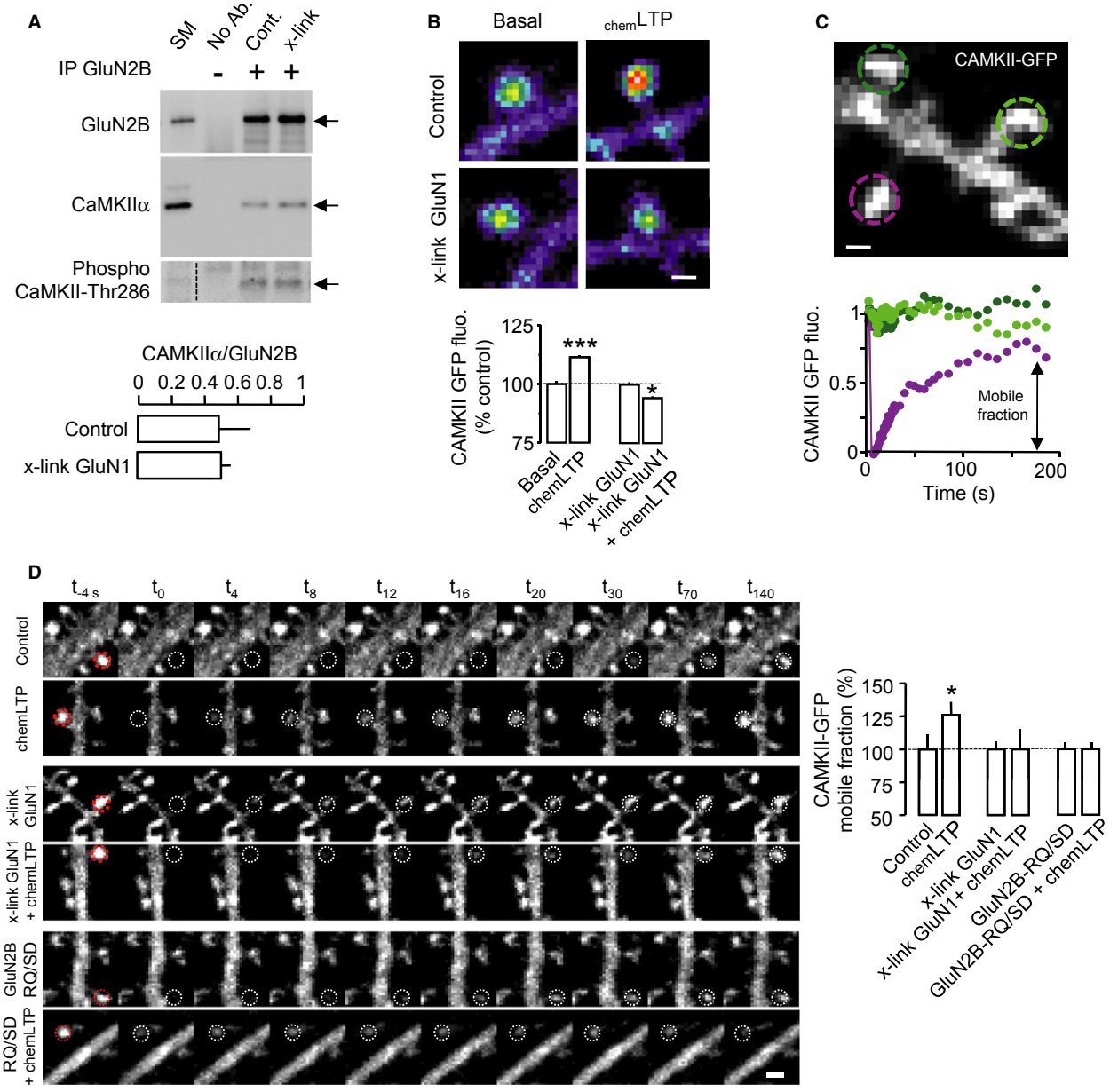

Figure 8. The activity-dependent shift in CaMKII dynamics within dendritic spines is regulated by GluN2B-NMDAR dynamics.

A Representative immunoblots showing the immunoprecipitation (IP) of CaMKII (α form) and phospho-CaMKII-Thr286 with GluN2B in membrane fractions from hippocampal slices (P17–20 rats) incubated with buffer (control) or GluN1 x-link. Lower panel: the ratio between CaMKII and GluN2B optical densities is represented (n = 3 independent experiments). SM, start material; No Ab., no antibody; Cont., control.

B CaMKII-GFP was detected and imaged in spines before (basal) and after $_{chem}$LTP in control and GluN1x-link conditions. Scale bar = 1 μm. Lower panel: CaMKII-GFP fluorescence intensity was compared between these conditions (basal: n = 6 neuronal fields, N = 765 spines; $_{chem}$LTP: n = 11 neuronal fields, N = 1,688 spines; basal versus $_{chem}$LTP, Student's t-test, ***$P < 0.0001$; x-link GluN1: n = 7 neuronal fields, N = 955 spines; x-link GluN1+$_{chem}$LTP: n = 9 neuronal fields, N = 1,728 spines; x-link GluN1 versus x-link GluN1+$_{chem}$LTP, Student's t-test, *$P < 0.05$).

C Time-lapse imaging of CaMKII-GFP in hippocampal dendritic spines in basal (light and dark green dotted circles) or FRAP (purple dotted circle) conditions. Scale bar = 1 μm. Lower panel: the fluorescence intensity was measured and plotted over time. CaMKII-GFP fluorescence was stable over time in basal condition. Note the recovery after photobleaching of the CaMKII-GFP fluorescence up to nearly 60% of its initial value, indicating a 60% mobile fraction.

D FRAP imaging of CaMKII-GFP in control, $_{chem}$LTP, GluN1 x-link, GluN1 x-link +$_{chem}$LTP, GluN2B-RQ/SD, and GluN2B-RQ/SD + $_{chem}$LTP conditions. Scale bar = 2 μm. The dotted line circles represent the photobleached areas. Time (t) is expressed in seconds. Right panel: normalized variation of the CaMKII-GFP mobile fraction in basal (n = 6 dendritic fields), $_{chem}$LTP (n = 10 dendritic fields, Student's t-test, *$P < 0.05$ compared to control), GluN1 x-link (black, n = 6 dendritic fields), GluN1 x-link+$_{chem}$LTP (n = 11 dendritic fields, Student's t-test, $P > 0.05$ when compared to GluN1 x-link), GluN2B-RQ/SD (n = 9 dendritic fields), and GluN2B-RQ/SD+$_{chem}$LTP (Student t-test n = 19 dendritic fields, Student's t-test, $P > 0.05$ when compared to GluN2B-RQ/SD) conditions.

Data information: Bars in bar graphs represent mean ± s.e.m.
Source data are available online for this figure.

altered by $_{chem}$LTP, we next investigated the dynamics of a PDZ-containing scaffold protein, that is, PSD-95, which physically binds NMDAR to stabilize them at the synapse (Bard *et al*, 2010). We found that $_{chem}$LTP does not change the mobile fraction of PSD-95, either in basal condition or in the presence of GluN1 x-link (Supplementary Fig S6B). Thus, contrary to CaMKII, PSD-95 trafficking within spines is not linked to the surface diffusion of NMDAR. Collectively, these data demonstrate that there is a functional link between the dynamics of surface NMDAR and intracellular CaMKII during synaptic plasticity. In addition to the well-described role of the enzymatic activity of CaMKII in the induction of LTP (Bayer *et al*, 2006; Sanhueza *et al*, 2011; Halt *et al*, 2012; Lisman *et al*, 2012), we now provide the first evidence that through their physical interaction, modifications of NMDAR surface dynamics directly impact on the trafficking and subcellular localization of CaMKII, thereby affecting the plastic range of synapses.

Discussion

Using a combination of high-resolution single nanoparticle tracking, bulk imaging, and electrophysiological approaches, we here demonstrate that acute changes in the GluN2B-NMDAR surface dynamics regulate LTP at glutamatergic synapses in maturing hippocampal neurons. During LTP, we have observed an NMDAR-, CaMKII-, and CKII-dependent fast lateral escape of synaptic GluN2B-NMDAR. Preventing this surface relocation i) alters the activity-dependent change in CaMKII intracellular dynamics in spines, which is operated by the direct interaction between GluN2B subunit and CaMKII, and ii) prevents LTP at glutamatergic synapses from immature hippocampal networks. Together, these data provide the first evidence for a non-canonical and key role of GluN2B-NMDAR surface dynamics in controlling the adaptation of glutamatergic synapses in the young hippocampus (Fig 9).

Although rapid changes in postsynaptic glutamate receptors, such as AMPAR, have been observed during long-term synaptic plasticity, NMDAR were considered to be highly stable during synaptic rearrangements (Malinow & Malenka, 2002). This view was, however, challenged by several reports showing that the NMDAR signaling slowly changed, in the hour range, during long-term synaptic plasticity processes such as LTP (Muller & Lynch, 1988; Bashir *et al*, 1991; Berretta *et al*, 1991; Xie *et al*, 1992; O'Connor *et al*, 1994; Xiao *et al*, 1995; Grosshans *et al*, 2002; Watt *et al*, 2004; Morishita *et al*, 2005; Harney *et al*, 2008; Harnett *et al*, 2009). This slow, long-term change in NMDAR signaling has been proposed, for instance, to contribute to the maintenance of the synaptic homeostasis after the AMPAR transmission increase (Watt *et al*, 2004), or to the control of the metaplastic range of synapses by spatially and locally adjusting the GluN2B-NMDAR content (Kwon & Castillo, 2008; Rebola *et al*, 2008, 2011; Ireland & Abraham, 2009; Lee *et al*, 2010). Rapid changes in NMDAR signaling have also been observed following LTP induction in the hippocampus (Bellone & Nicoll, 2007). In the CA1 area of neonatal rats, the GluN2A/2B-NMDAR synaptic ratio rapidly increases after LTP induction through a decreased contribution of synaptic GluN2B-NMDAR (Bellone & Nicoll, 2007). Taking advantage of the high pointing accuracy (~20–30 nm) of the single nanoparticle approach, we here provide the first evidence that LTP induction is indeed associated with a local and rapid lateral redistribution of surface GluN2B-NMDAR. The specific involvement of the GluN2B-NMDAR subtype is fully consistent with its high surface dynamics when compared to GluN2A-NMDAR (Groc *et al*, 2006). It is also in line with its higher content in the periphery of the postsynaptic areas (Shinohara *et al*, 2008), a strategic location from where it can be rapidly trafficked from/toward the postsynaptic density. The dynamic properties of surface GluN2B-NMDAR thus represent an additional molecular mechanism controlling the adaptation of glutamatergic synapses in immature neurons. Since the number of NMDAR in the hippocampal CA1 area is in the range of 20–50 per synapse (Shinohara *et al*, 2008), a lateral redistribution of only 4–10 NMDAR (~20% reduction) could profoundly alter the plastic range of a given synapse, likely through changes in GluN2-NMDAR-dependent calcium transients and their related signaling cascades in the spine (Sobczyk *et al*, 2005; Sobczyk & Svoboda, 2007). This is further consistent with data suggesting that a 20–30% reduction in the availability of synaptic NMDAR due to reduced occupancy of the NMDAR co-agonist site can block LTP induction (Henneberger *et al*, 2010). Finally, an exciting study demonstrated that ligand binding to NMDAR is sufficient to induce synaptic long-term depression in cation flow- and Ca^{2+}-independent manner (Nabavi *et al*, 2013).

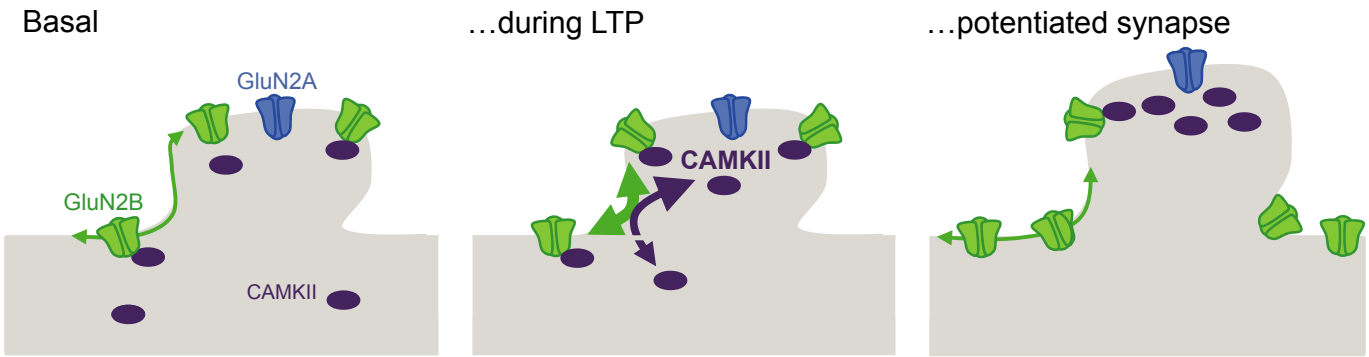

Figure 9. Schematic model of the dynamic interplay between surface GluN2B-NMDAR and CaMKII during synaptic long-term potentiation (LTP).
In basal conditions, GluN2B-NMDAR surface diffusion is regulated by the activity of CaMKII. During activity-dependent changes in glutamatergic synaptic transmission, increased surface dynamics of GluN2B-NMDAR favors the intracellular redistribution of CaMKII through their direct interaction, promoting the accumulation of CaMKII in spines.

Considering that impairing the activity-elicited surface redistribution of GluN2B-NMDAR without affecting NMDAR-mediated synaptic currents or calcium influx was sufficient to prevent LTP, NMDAR surface dynamics clearly emerges as a key controller of glutamate synapse plastic range.

Although the complete molecular cascade remains to be determined, we show that changes in GluN2B-NMDAR surface dynamics underlie the activity-dependent recruitment and accumulation of CaMKII to the postsynaptic compartment, a process that requires the direct interaction between GluN2B subunit and CAMKII. We propose that, following NMDAR activation in immature neurons, CaMKII binds GluN2B-NMDAR and rapidly increases its lateral diffusion in the spine area. This in turn functionally impacts on the intracellular dynamics and redistribution of CaMKII from the dendritic shaft to the postsynaptic compartment, providing a rapid and efficient way to modulate the spine content in CaMKII. In addition, we show that the dynamic remodeling of GluN2B-NMDAR following LTP depends on both CaMKII and CKII activation. This is fully consistent with recent studies showing that CKII is directly involved in the GluN2B to GluN2A subunit switch during development and plasticity through an active interplay with CaMKII (Sanz-Clemente *et al*, 2010, 2013; Matta *et al*, 2011). It should, however, be mentioned that both PKA and PKC have been previously involved in the plasticity of glutamate synapses, and the fact that they do not participate in the LTP-induced lateral redistribution of GluN2B-NMDAR simply indicates that under our specific conditions (e.g., developmental stage, neuronal preparation), they are not the drive controlling the relocation of surface NMDAR. At this point, we cannot exclude that other protein kinases and signaling cascades may participate in the synaptic redistribution of NMDAR. Additional studies investigating whether the developmental stage, the brain area, or the activity pattern differentially affects protein kinase recruitment and GluN2-NMDAR surface dynamics will be of particular interest.

In mature neurons, the absence of change in GluN2B-NMDAR surface dynamics during LTP and the modest effect of GluN1 x-link on LTP at CA3-CA1 synapses indicate that NMDAR surface dynamics play different roles in immature and mature hippocampal networks. This observation is consistent with electrophysiological recordings at CA3-CA1 synapses showing that activity-dependent changes in NMDAR signaling are only observed in neonatal rats (Bellone & Nicoll, 2007). Together with the fact that NMDAR-dependent LTP in the developing and mature brains shares similar induction conditions but displays clear discrepancies (e.g., protein kinase required, synapse unsilencing, GluA subunit trafficking) (Durand *et al*, 1996; Isaac *et al*, 1997; Zhu *et al*, 2000; Liao *et al*, 2001; Yasuda *et al*, 2003; Abrahamsson *et al*, 2008), our present data suggest that the rapid lateral mobilization of surface GluN2B-NMDAR during developmental LTP in the hippocampus is a novel feature of immature synapses. During the postnatal period in the hippocampus, the number of mature glutamate synapses steadily increases, mostly due to the incorporation/stabilization of AMPAR at immature synapses (Durand *et al*, 1996; Hsia *et al*, 1998; Yasuda *et al*, 2003; Abrahamsson *et al*, 2008). Interestingly, the surface diffusion of NMDAR changes during development as exhibited by the lower dynamic retention of GluN2B-NMDAR (i.e., synaptic dwell-time) in the area of mature synapses (Tovar & Westbrook, 2002; Groc *et al*, 2006). The maturation of glutamatergic synapses is thus paralleled by a shift in the surface dynamics of GluN2B-NMDAR, eventually leading to a reduced lateral mobility of receptors in mature synapses (Hanse *et al*, 2009). At the molecular level, one may expect that the machineries controlling GluN2B-NMDAR surface dynamics and synaptic anchorage are also developmentally regulated. Interestingly, the extracellular protein reelin which is expressed early in the development and supports synaptic maturation and plasticity (Frotscher, 2010) strongly and specifically regulates GluN2B-NMDAR surface trafficking (Groc *et al*, 2007a). Furthermore, PSD proteins such as PSD95 and SAP102 (Bard *et al*, 2010), extracellular matrix compounds such as matrix metalloproteases (Michaluk *et al*, 2009), or co-agonists such as D-serine and glycine (Papouin *et al*, 2012) are established modulators of NMDAR surface trafficking and developmental maturation of glutamate synapses. Finally, the presence of a substantial amount of triheteromeric GluN1/2A/2B-NMDAR in mature glutamate synapses (Sheng *et al*, 1994; Gray *et al*, 2011; Rauner & Kohr, 2011; Tovar *et al*, 2013) may add another layer of complexity to the activity-dependent regulation of NMDAR surface dynamics. Investigating the precise mechanisms controlling GluN2B-NMDAR surface trafficking during synaptic plasticity and testing whether these processes could be reinitiated in mature networks will be of particular interest.

The requirement for NMDAR activation in the establishment of learning and memory functions in rodents has been extensively reported over the last decades, starting from the second half of the first postnatal month. In humans however, this exploration has been limited by the lack of non-invasive methods and our knowledge of NMDAR function mostly relies on the psychiatric symptoms observed in patients under NMDAR-related drugs of abuse (e.g., PCP, ketamine). Using purified anti-NMDAR autoantibodies from patients suffering autoimmune encephalitis, we here provide evidence that human antibodies affect the surface dynamics of NMDAR and thereby prevent LTP expression in hippocampal neurons. Consistent with the role of NMDAR-dependent LTP in learning and memory, patients expressing these autoantibodies suffer from short-term memory deficits that disappear upon antibody dialysis. Since it contributes to the regulation of synaptic adaptations in physiological conditions, NMDAR surface dynamics could constitute a potential therapeutic target in brain dysfunctions involving synaptic plasticity deficits. Consistently, it has been recently shown that Aβ-induced synaptic signaling dysfunction is mediated by a non-canonical, ion flux-independent alteration of NMDAR (Kessels *et al*, 2013). Investigating the potential alterations of NMDAR surface trafficking and conformation in neuropsychiatric disorders such as neurodegenerative diseases or schizophrenia could thus help us shed new lights on the relationship between receptor surface dynamics and neuronal network pathophysiology.

Materials and Methods

Cell culture, protein expression, synaptic live staining, and immunocytochemistry

Cultures of hippocampal neurons were prepared from E18 Sprague-Dawley rats following a previously described method (Mikasova *et al*, 2012). Briefly, cells were plated at a density of 200-300 × 10^3 cells per dish on poly-lysine-pre-coated coverslips. Coverslips were

maintained in a 3% serum-containing neurobasal medium. This medium was replaced after 4 days *in vitro* (div) by a serum-free neurobasal medium and kept as previously indicated. Cultures were kept at 37°C in 5% CO_2 for 20 div at maximum. For live imaging, neurons were transfected with GluN1-SEP, GluN2B-SEP, CaMKII-GFP, PSD-95-GFP, or Homer 1c-DsRed at 7–14 div using the Effecten transfection. To label synapses, the postsynaptic marker Homer 1c-GFP or DsRed was expressed alone (for QD experiments) or co-expressed with GluA1-SEP or GluN1-SEP for the time-lapse and FRAP experiments. The vast majority of Homer 1c-GFP clusters co-localize with pre-synaptic markers (Ehlers *et al*, 2007). To express GluN2B-SEP in organotypic slices, we used a gene-gun biolistic approach in 8-10 div cultured slices. For immunostaining, surface GluA2-AMPAR were specifically stained using a monoclonal anti-GluA2 subunit antibody (1:100) for 15 min on live neurons at 37°C in culture medium. For the quantification of surface AMPAR staining within individual synapses, the Shank (1:1,000 primary antibody) staining served as a mask filter to isolate surface GluA2 subunit staining in individual Shank clusters. The integrated fluorescence level over the Shank cluster area was then measured for each cluster. The fluorescence analysis was performed using imaging tools from Metamorph software (Universal Imaging Corporation, PA, USA).

Single quantum dot tracking and surface diffusion

As previously described (Groc *et al*, 2004, 2006, 2007b; Bats *et al*, 2007; Heine *et al*, 2008), quantum dots (QD) 655 goat $F(ab')_2$ anti-rabbit IgG (Invitrogen) were first incubated for 30 min with 1 μl of the polyclonal antibodies against GluN2A (Alomone Labs; epitope corresponding to residues 41–53 of GluN2A subunit) or GluN2B subunits (Alomone Labs; epitope corresponding to residues 323–337 of GluN2B subunit). Images were obtained with an acquisition time of 50 ms with up to 1,000 consecutive frames. Signals were detected using an EMCCD camera (Quantem, Roper Scientific). The instantaneous diffusion coefficient "D" was calculated for each trajectory, from linear fits of the first four points of the mean square displacement versus time function using $MSD(t) = < r^2 > (t) = 4Dt$. To determine the distribution and synaptic fraction of single QD complexes, frame stacks were obtained and on each frame the receptor/particle complexes were precisely located in synaptic, perisynaptic, and extrasynaptic compartments. Then, those locations were projected on a single image, providing a high-resolution distribution of the receptor/QD complexes.

Fluorescent recovery after photobleaching and cluster fluorescence intensity

GluN1-SEP, GluN2B-SEP, GluA1-SEP, CaMKII-GFP, PSD-95-GFP, and/or Homer 1c-DsRed co-transfected neurons were imaged on an inverted confocal spinning-disk microscope (Leica). Fluorescence was excited using a monochromator controlled by Metamorph software (Universal Imaging, USA). To photobleach locally, we used a Saphire laser 488 nm at 50% power to avoid photodamage. Recovery from photobleaching was monitored by three consecutive acquisition periods at 2-, 0.5-, and 0.1-Hz acquisition rates, respectively. Clusters were imaged over a period of 30 min. Fluorescence intensity was measured using Metamorph software (universal imaging, USA) and corrected for photobleaching and background noise.

Chemically induced potentiation ($_{chem}$LTP) and cross-link (x-link) protocol

As previously described (Lu *et al*, 2001; Park *et al*, 2004, 2006; Wang *et al*, 2008), chemically induced long-term potentiation ($_{chem}$LTP) was elicited by a bath co-application of glycine (200 μM) and picrotoxin (5 μM) for 4 min. For some experiments, chemically induced LTP was elicited by a similar bath co-application of forskolin (50 μM), rolipram (100 nM), and picrotoxin (5 μM). In all live experiments, $_{chem}$LTP was always applied after a period of baseline acquisition and the medium was carefully replaced by fresh equilibrated and heated medium after induction. As previously described (Groc *et al*, 2008; Heine *et al*, 2008), for the x-link experiments, neurons were co-transfected with GluN1-SEP or GluN2B-SEP and Homer 1c-DsRed and incubated with highly concentrated (1:20) polyclonal antibodies directed against GluN1 (Alomone Labs; epitope corresponding to residues 385–399 of the GluN1 subunit), GluN2B (Alomone Labs; same as above), GluN2A (Alomone Labs; same as above) NMDAR subunits or against GFP (Chemicon). For autoimmune anti-NMDAR antibodies, cerebrospinal fluid was obtained from different patients with typical encephalitis with antibodies to GluN1/GluN2 heteromers of the NMDAR (see for details, Mikasova *et al*, 2012), and IgG were purified (concentration 2 mg/ml) as previously described (Manto *et al*, 2007).

In vivo hippocampal injection

Briefly, P10-15 Sprague-Dawley rats were anesthetized by inhalation of isoflurane. The stereotaxic coordinates for the injection of anti-NMDAR antibodies in the dorsal hippocampus were adapted according to the age of the animals (coordinates relative to bregma, from AP: −3 mm, ML: ± 1.8 mm, DV: −2 mm at P10, to AP: −4.5 mm, ML: ± 2.2 mm, DV: −2.5 mm at P15). A total of 500–1,000 nl of anti-NMDAR antibodies dissolved in a PBS solution was injected per brain hemisphere.

Electrophysiology

Patch-clamp recordings. For cultured hippocampal neuron recordings, cells were transferred to a recording chamber and continuously superfused with an external solution heated to 37°C and containing (in mM): 145 NaCl, 2.5 KCl, 10 HEPES, 10 D-glucose, 2 $MgCl_2$, and 2 $CaCl_2$ adjusted to pH 7.4 with NaOH. Electrodes (4–5 MΩ) were filled with a solution containing the following (in mM): 125 cesium methanesulfonate, 2 $MgCl_2$, 1 $CaCl_2$, 10 HEPES, 10 EGTA, 4 Na2ATP, 0.4 Na3GTP, and 5 QX-314 adjusted to pH 7.25 with CsOH. Spontaneous NMDA-mediated excitatory postsynaptic currents (sEPSCs) were recorded at +40 mV in the presence of the $GABA_A$ receptor antagonist bicuculline (20 μM) and the AMPA receptor antagonist NBQX (10 μM; Sigma-Aldrich, St. Louis, MO). For CA1 patch-clamp recordings, P10–15 Sprague-Dawley rats were anesthetized with isoflurane and parasagittal brain slices (350-μm thick) were prepared and stored at room temperature in an artificial CSF (ACSF) solution containing (in mM): 126 NaCl, 3.5 KCl, 2 $CaCl_2$, 1.3 $MgCl_2$, 1.2 NaH_2PO_4, 25 $NaHCO_3$, and 12.1 glucose (gassed with

95% O_2/5% CO_2; pH 7.35). Electrodes (4–5 MΩ) were filled with a solution containing (in mM): 120 cesium methanesulfonate, 4 NaCl, 4 $MgCl_2$, 10 HEPES, 0.2 EGTA, 4 Na2ATP, 0.33 Na3GTP, and 5 phosphocreatine adjusted to pH 7.3 with CsOH. EPSCs were evoked at a rate of 0.05 Hz using an ACSF-filled glass microelectrode positioned in the stratum radiatum to stimulate Schaffer collaterals. Currents were recorded in the presence of bicuculline (20 μM) in order to block $GABA_A$ receptors. LTP was induced by a pairing protocol consisting of 200 Schaffer collateral stimulations at 2 Hz while depolarizing the postsynaptic cell to −5 mV. The access resistance was monitored throughout the experiment, and data were discarded when it changed by > 20%.

fEPSP recordings. Hippocampal slices were prepared from P15 to 17 Wistar rats. fEPSP were evoked alternately at 0.1 Hz at two independent synaptic inputs in the CA1 stratum radiatum. LTP was induced by a 20-impulse 100-Hz train repeated five times with 10 s between trains. GABAergic inhibition was blocked by picrotoxin (100 μM).

Co-immunoprecipitation and western blot

P2 crude membrane fractions were prepared from hippocampal slices of P17–20 Sprague–Dawley rats obtained as described above. P2 pellets were solubilized with a Triton buffer and 100–150 g of total protein was incubated with protein A coated with an anti-GluN2B antibody overnight at 4°C. After a 5-min denaturation step at 95°C, samples (without beads) were separated by SDS–PAGE and blotted onto a nitrocellulose membrane. After blocking, membranes were hybridized with an anti-GluN2B antibody (1:2,000, Rabbit polyclonal Ab, Molecular Probes), an anti-CaMKII antibody (1:200, Santa Cruz), or an anti-phospho-CaMKII (Thr 286) antibody (1:1,000, Millipore). Detection was performed using the SuperSignal West Femto Maximum Sensitivity Substrate detection System (Pierce) revealed with a Chemigenius system (Syngene). Quantification of band intensity was performed using Genetools software (Syngene).

Supplementary information for this article is available online: http://emboj.embopress.org

Acknowledgements

This work was supported by the Centre National de la Recherche Scientifique, Agence Nationale de la Recherche, Fondation pour la Recherche Médicale, Conseil Régional d'Aquitaine, Labex Bordeaux BRAIN, and Ministère de l'Enseignement supérieur et de la Recherche. We thank Stéphane Oliet, Pierre Paoletti, and Dmitri A. Rusakov for constructive discussions and critical reading of the manuscript. We thank the Bordeaux Imaging Center and Jean-Baptiste Sibarita for technical support. We also thank Andres Barria for GluN2B subunit constructs, Olivier Nicole for CaMKII antibody, Christelle Breillat, Aurélia Ledantec for technical assistance on cell cultures, and laboratory members for constructive discussions.

Author contributions

LG, JPD, and LL designed the research. JPD, LL, HS, LB, JV, LM, DB, and EH performed experiments and analysis. VR and JH provided reagents. LG, JPD, and LL wrote the manuscript.

Conflict of interest

The authors declare that they have no conflict of interest.

References

Abrahamsson T, Gustafsson B, Hanse E (2008) AMPA silencing is a prerequisite for developmental long-term potentiation in the hippocampal CA1 region. *J Neurophysiol* 100: 2605 – 2614

Ashby MC, Maier SR, Nishimune A, Henley JM (2006) Lateral diffusion drives constitutive exchange of AMPA receptors at dendritic spines and is regulated by spine morphology. *J Neurosci* 26: 7046 – 7055

Bard L, Sainlos M, Bouchet D, Cousins S, Mikasova L, Breillat C, Stephenson FA, Imperiali B, Choquet D, Groc L (2010) Dynamic and specific interaction between synaptic NR2-NMDA receptor and PDZ proteins. *Proc Natl Acad Sci USA* 107: 19561 – 19566

Barria A, Malinow R (2005) NMDA receptor subunit composition controls synaptic plasticity by regulating binding to CaMKII. *Neuron* 48: 289 – 301

Bashir ZI, Alford S, Davies SN, Randall AD, Collingridge GL (1991) Long-term potentiation of NMDA receptor-mediated synaptic transmission in the hippocampus. *Nature* 349: 156 – 158

Bats C, Groc L, Choquet D (2007) The interaction between Stargazin and PSD-95 regulates AMPA receptor surface trafficking. *Neuron* 53: 719 – 734

Bayer KU, De Koninck P, Leonard AS, Hell JW, Schulman H (2001) Interaction with the NMDA receptor locks CaMKII in an active conformation. *Nature* 411: 801 – 805

Bayer KU, LeBel E, McDonald GL, O'Leary H, Schulman H, De Koninck P (2006) Transition from reversible to persistent binding of CaMKII to postsynaptic sites and NR2B. *J Neurosci* 26: 1164 – 1174

Bellone C, Nicoll RA (2007) Rapid bidirectional switching of synaptic NMDA receptors. *Neuron* 55: 779 – 785

Berretta N, Berton F, Bianchi R, Brunelli M, Capogna M, Francesconi W (1991) Long-term Potentiation of NMDA receptor-mediated EPSP in Guinea-pig Hippocampal Slices. *Eur J Neurosci* 3: 850 – 854

Chapman MR, Vause HE (2011) Anti-NMDA receptor encephalitis: diagnosis, psychiatric presentation, and treatment. *Am J Psychiatry* 168: 245 – 251

Chen BS, Roche KW (2007) Regulation of NMDA receptors by phosphorylation. *Neuropharmacology* 53: 362 – 368

Collingridge GL, Isaac JT, Wang YT (2004) Receptor trafficking and synaptic plasticity. *Nat Rev Neurosci* 5: 952 – 962

Cull-Candy S, Brickley S, Farrant M (2001) NMDA receptor subunits: diversity, development and disease. *Curr Opin Neurobiol* 11: 327 – 335

Cull-Candy SG, Leszkiewicz DN (2004) Role of distinct NMDA receptor subtypes at central synapses. *Sci STKE* 2004: re16

Dahan M, Levi S, Luccardini C, Rostaing P, Riveau B, Triller A (2003) Diffusion dynamics of glycine receptors revealed by single-quantum dot tracking. *Science* 302: 442 – 445

Dalmau J, Gleichman AJ, Hughes EG, Rossi JE, Peng X, Lai M, Dessain SK, Rosenfeld MR, Balice-Gordon R, Lynch DR (2008) Anti-NMDA-receptor encephalitis: case series and analysis of the effects of antibodies. *Lancet Neurol* 7: 1091 – 1098

Dalmau J, Lancaster E, Martinez-Hernandez E, Rosenfeld MR, Balice-Gordon R (2011) Clinical experience and laboratory investigations in patients with anti-NMDAR encephalitis. *Lancet Neurol* 10: 63 – 74

Dalmau J, Tuzun E, Wu HY, Masjuan J, Rossi JE, Voloschin A, Baehring JM, Shimazaki H, Koide R, King D, Mason W, Sansing LH, Dichter MA, Rosenfeld MR, Lynch DR (2007) Paraneoplastic anti-N-methyl-D-aspartate receptor encephalitis associated with ovarian teratoma. *Ann Neurol* 61: 25 – 36

Durand GM, Kovalchuk Y, Konnerth A (1996) Long-term potentiation and functional synapse induction in developing hippocampus. *Nature* 381: 71 – 75

Ehlers MD, Heine M, Groc L, Lee MC, Choquet D (2007) Diffusional trapping of GluR1 AMPA receptors by input-specific synaptic activity. *Neuron* 54: 447–460

Frotscher M (2010) Role for reelin in stabilizing cortical architecture. *Trends Neurosci* 33: 407–414

Gleichman AJ, Spruce LA, Dalmau J, Seeholzer SH, Lynch DR (2012) Anti-NMDA receptor encephalitis antibody binding is dependent on amino acid identity of a small region within the GluN1 amino terminal domain. *J Neurosci* 32: 11082–11094

Gray JA, Shi Y, Usui H, During MJ, Sakimura K, Nicoll RA (2011) Distinct modes of AMPA receptor suppression at developing synapses by GluN2A and GluN2B: single-cell NMDA receptor subunit deletion *in vivo*. *Neuron* 71: 1085–1101

Groc L, Choquet D (2008) Measurement and characteristics of neurotransmitter receptor surface trafficking (Review). *Mol Membr Biol* 25: 344–352

Groc L, Choquet D, Chaouloff F (2008) The stress hormone corticosterone conditions AMPAR surface trafficking and synaptic potentiation. *Nat Neurosci* 11: 868–870

Groc L, Choquet D, Stephenson FA, Verrier D, Manzoni OJ, Chavis P (2007a) NMDA receptor surface trafficking and synaptic subunit composition are developmentally regulated by the extracellular matrix protein Reelin. *J Neurosci* 27: 10165–10175

Groc L, Heine M, Cognet L, Brickley K, Stephenson FA, Lounis B, Choquet D (2004) Differential activity-dependent regulation of the lateral mobilities of AMPA and NMDA receptors. *Nat Neurosci* 7: 695–696

Groc L, Heine M, Cousins SL, Stephenson FA, Lounis B, Cognet L, Choquet D (2006) NMDA receptor surface mobility depends on NR2A-2B subunits. *Proc Natl Acad Sci USA* 103: 18769–18774

Groc L, Lafourcade M, Heine M, Renner M, Racine V, Sibarita JB, Lounis B, Choquet D, Cognet L (2007b) Surface trafficking of neurotransmitter receptor: comparison between single-molecule/quantum dot strategies. *J Neurosci* 27: 12433–12437

Grosshans DR, Clayton DA, Coultrap SJ, Browning MD (2002) LTP leads to rapid surface expression of NMDA but not AMPA receptors in adult rat CA1. *Nat Neurosci* 5: 27–33

Halt AR, Dallapiazza RF, Zhou Y, Stein IS, Qian H, Juntti S, Wojcik S, Brose N, Silva AJ, Hell JW (2012) CaMKII binding to GluN2B is critical during memory consolidation. *EMBO J* 31: 1203–1216

Hanse E, Taira T, Lauri S, Groc L (2009) Glutamate synapse in developing brain: an integrative perspective beyond the silent state. *Trends Neurosci* 32: 532–537

Harnett MT, Bernier BE, Ahn KC, Morikawa H (2009) Burst-timing-dependent plasticity of NMDA receptor-mediated transmission in midbrain dopamine neurons. *Neuron* 62: 826–838

Harney SC, Jane DE, Anwyl R (2008) Extrasynaptic NR2D-containing NMDARs are recruited to the synapse during LTP of NMDAR-EPSCs. *J Neurosci* 28: 11685–11694

Harris AZ, Pettit DL (2007) Extrasynaptic and synaptic NMDA receptors form stable and uniform pools in rat hippocampal slices. *J Physiol* 584(Pt 2): 509–519

Heine M, Groc L, Frischknecht R, Beique JC, Lounis B, Rumbaugh G, Huganir RL, Cognet L, Choquet D (2008) Surface mobility of postsynaptic AMPARs tunes synaptic transmission. *Science* 320: 201–205

Henneberger C, Papouin T, Oliet SH, Rusakov DA (2010) Long-term potentiation depends on release of D-serine from astrocytes. *Nature* 463: 232–236

Hsia AY, Malenka RC, Nicoll RA (1998) Development of excitatory circuitry in the hippocampus. *J Neurophysiol* 79: 2013–2024

Hughes EG, Peng X, Gleichman AJ, Lai M, Zhou L, Tsou R, Parsons TD, Lynch DR, Dalmau J, Balice-Gordon RJ (2010) Cellular and synaptic mechanisms of anti-NMDA receptor encephalitis. *J Neurosci* 30: 5866–5875

Ireland DR, Abraham WC (2009) Mechanisms of group I mGluR-dependent long-term depression of NMDA receptor-mediated transmission at Schaffer collateral-CA1 synapses. *J Neurophysiol* 101: 1375–1385

Isaac JTR, Crair MC, Nicoll RA, Malenka RC (1997) Silent synapses during development of thalamocortical inputs. *Neuron* 18: 269–280

Ito I, Kawakami R, Sakimura K, Mishina M, Sugiyama H (2000) Input-specific targeting of NMDA receptor subtypes at mouse hippocampal CA3 pyramidal neuron synapses. *Neuropharmacology* 39: 943–951

Kawakami R, Shinohara Y, Kato Y, Sugiyama H, Shigemoto R, Ito I (2003) Asymmetrical allocation of NMDA receptor epsilon2 subunits in hippocampal circuitry. *Science* 300: 990–994

Kessels HW, Nabavi S, Malinow R (2013) Metabotropic NMDA receptor function is required for beta-amyloid-induced synaptic depression. *Proc Natl Acad Sci USA* 110: 4033–4038

Kwon HB, Castillo PE (2008) Long-term potentiation selectively expressed by NMDA receptors at hippocampal mossy fiber synapses. *Neuron* 57: 108–120

Lau CG, Zukin RS (2007) NMDA receptor trafficking in synaptic plasticity and neuropsychiatric disorders. *Nat Rev Neurosci* 8: 413–426

Lee JY, Huerta PT, Zhang J, Kowal C, Bertini E, Volpe BT, Diamond B (2009) Neurotoxic autoantibodies mediate congenital cortical impairment of offspring in maternal lupus. *Nat Med* 15: 91–96

Lee MC, Yasuda R, Ehlers MD (2010) Metaplasticity at single glutamatergic synapses. *Neuron* 66: 859–870

Liao D, Scannevin RH, Huganir R (2001) Activation of silent synapses by rapid activity-dependent synaptic recruitment of AMPA receptors. *J Neurosci* 21: 6008–6017

Lisman J, Schulman H, Cline H (2002) The molecular basis of CaMKII function in synaptic and behavioural memory. *Nat Rev Neurosci* 3: 175–190

Lisman J, Yasuda R, Raghavachari S (2012) Mechanisms of CaMKII action in long-term potentiation. *Nat Rev Neurosci* 13: 169–182

Lu J, Helton TD, Blanpied TA, Racz B, Newpher TM, Weinberg RJ, Ehlers MD (2007) Postsynaptic positioning of endocytic zones and AMPA receptor cycling by physical coupling of dynamin-3 to Homer. *Neuron* 55: 874–889

Lu KT, Gean PW (1999) Masking of forskolin-induced long-term potentiation by adenosine accumulation in area CA1 of the rat hippocampus. *Neuroscience* 88: 69–78

Lu W, Man H, Ju W, Trimble WS, MacDonald JF, Wang YT (2001) Activation of synaptic NMDA receptors induces membrane insertion of new AMPA receptors and LTP in cultured hippocampal neurons. *Neuron* 29: 243–254

Malinow R, Malenka RC (2002) AMPA receptor trafficking and synaptic plasticity. *Annu Rev Neurosci* 25: 103–126

Manto MU, Laute MA, Aguera M, Rogemond V, Pandolfo M, Honnorat J (2007) Effects of anti-glutamic acid decarboxylase antibodies associated with neurological diseases. *Ann Neurol* 61: 544–551

Matta JA, Ashby MC, Sanz-Clemente A, Roche KW, Isaac JT (2011) mGluR5 and NMDA receptors drive the experience- and activity-dependent NMDA receptor NR2B to NR2A subunit switch. *Neuron* 70: 339–351

Michaluk P, Mikasova L, Groc L, Frischknecht R, Choquet D, Kaczmarek L (2009) Matrix metalloproteinase-9 controls NMDA receptor surface diffusion through integrin beta1 signaling. *J Neurosci* 29: 6007–6012

Mikasova L, De Rossi P, Bouchet D, Georges F, Rogemond V, Didelot A, Meissirel C, Honnorat J, Groc L (2012) Disrupted surface cross-talk between NMDA and Ephrin-B2 receptors in anti-NMDA encephalitis. *Brain* 135(Pt 5): 1606 – 1621

Morishita W, Marie H, Malenka RC (2005) Distinct triggering and expression mechanisms underlie LTD of AMPA and NMDA synaptic responses. *Nat Neurosci* 8: 1043 – 1050

Moscato EH, Jain A, Peng X, Hughes EG, Dalmau J, Balice-Gordon RJ (2010) Mechanisms underlying autoimmune synaptic encephalitis leading to disorders of memory, behavior and cognition: insights from molecular, cellular and synaptic studies. *Eur J Neurosci* 32: 298 – 309

Muller D, Lynch G (1988) Long-term potentiation differentially affects two components of synaptic responses in hippocampus. *Proc Natl Acad Sci USA* 85: 9346 – 9350

Nabavi S, Kessels HW, Alfonso S, Aow J, Fox R, Malinow R (2013) Metabotropic NMDA receptor function is required for NMDA receptor-dependent long-term depression. *Proc Natl Acad Sci USA* 110: 4027 – 4032

O'Connor JJ, Rowan MJ, Anwyl R (1994) Long-lasting enhancement of NMDA receptor-mediated synaptic transmission by metabotropic glutamate receptor activation. *Nature* 367: 557 – 559

Otmakhov N, Khibnik L, Otmakhova N, Carpenter S, Riahi S, Asrican B, Lisman J (2004a) Forskolin-induced LTP in the CA1 hippocampal region is NMDA receptor dependent. *J Neurophysiol* 91: 1955 – 1962

Otmakhov N, Tao-Cheng JH, Carpenter S, Asrican B, Dosemeci A, Reese TS, Lisman J (2004b) Persistent accumulation of calcium/calmodulin-dependent protein kinase II in dendritic spines after induction of NMDA receptor-dependent chemical long-term potentiation. *J Neurosci* 24: 9324 – 9331

Papouin T, Ladepeche L, Ruel J, Sacchi S, Labasque M, Hanini M, Groc L, Pollegioni L, Mothet JP, Oliet SH (2012) Synaptic and extrasynaptic NMDA receptors are gated by different endogenous coagonists. *Cell* 150: 633 – 646

Park M, Penick EC, Edwards JG, Kauer JA, Ehlers MD (2004) Recycling endosomes supply AMPA receptors for LTP. *Science* 305: 1972 – 1975

Park M, Salgado JM, Ostroff L, Helton TD, Robinson CG, Harris KM, Ehlers MD (2006) Plasticity-induced growth of dendritic spines by exocytic trafficking from recycling endosomes. *Neuron* 52: 817 – 830

Petrini EM, Lu J, Cognet L, Lounis B, Ehlers MD, Choquet D (2009) Endocytic trafficking and recycling maintain a pool of mobile surface AMPA receptors required for synaptic potentiation. *Neuron* 63: 92 – 105

Rauner C, Kohr G (2011) Triheteromeric NR1/NR2A/NR2B receptors constitute the major N-methyl-D-aspartate receptor population in adult hippocampal synapses. *J Biol Chem* 286: 7558 – 7566

Rebola N, Carta M, Lanore F, Blanchet C, Mulle C (2011) NMDA receptor-dependent metaplasticity at hippocampal mossy fiber synapses. *Nat Neurosci* 14: 691 – 693

Rebola N, Lujan R, Cunha RA, Mulle C (2008) Adenosine A2A receptors are essential for long-term potentiation of NMDA-EPSCs at hippocampal mossy fiber synapses. *Neuron* 57: 121 – 134

Sanhueza M, Fernandez-Villalobos G, Stein IS, Kasumova G, Zhang P, Bayer KU, Otmakhov N, Hell JW, Lisman J (2011) Role of the CaMKII/NMDA receptor complex in the maintenance of synaptic strength. *J Neurosci* 31: 9170 – 9178

Sanz-Clemente A, Gray JA, Ogilvie KA, Nicoll RA, Roche KW (2013) Activated CaMKII couples GluN2B and casein kinase 2 to control synaptic NMDA receptors. *Cell Rep* 3: 607 – 614

Sanz-Clemente A, Matta JA, Isaac JT, Roche KW (2010) Casein kinase 2 regulates the NR2 subunit composition of synaptic NMDA receptors. *Neuron* 67: 984 – 996

Sharma K, Fong DK, Craig AM (2006) Postsynaptic protein mobility in dendritic spines: long-term regulation by synaptic NMDA receptor activation. *Mol Cell Neurosci* 31: 702 – 712

Shen K, Meyer T (1999) Dynamic control of CaMKII translocation and localization in hippocampal neurons by NMDA receptor stimulation. *Science* 284: 162 – 166

Sheng M, Cummings J, Roldan LA, Jan YN, Jan LY (1994) Changing subunit composition of heteromeric NMDA receptors during development of rat cortex. *Nature* 368: 144 – 147

Shinohara Y, Hirase H, Watanabe M, Itakura M, Takahashi M, Shigemoto R (2008) Left-right asymmetry of the hippocampal synapses with differential subunit allocation of glutamate receptors. *Proc Natl Acad Sci USA* 105: 19498 – 19503

Smith GB, Heynen AJ, Bear MF (2009) Bidirectional synaptic mechanisms of ocular dominance plasticity in visual cortex. *Philos Trans R Soc Lond B Biol Sci* 364: 357 – 367

Sobczyk A, Scheuss V, Svoboda K (2005) NMDA receptor subunit-dependent [$Ca2^{+}$] signaling in individual hippocampal dendritic spines. *J Neurosci* 25: 6037 – 6046

Sobczyk A, Svoboda K (2007) Activity-dependent plasticity of the NMDA-receptor fractional Ca2 + current. *Neuron* 53: 17 – 24

Strack S, Robison AJ, Bass MA, Colbran RJ (2000) Association of calcium/calmodulin-dependent kinase II with developmentally regulated splice variants of the postsynaptic density protein densin-180. *J Biol Chem* 275: 25061 – 25064

Tovar KR, McGinley MJ, Westbrook GL (2013) Triheteromeric NMDA receptors at hippocampal synapses. *J Neurosci* 33: 9150 – 9160

Tovar KR, Westbrook GL (2002) Mobile NMDA receptors at hippocampal synapses. *Neuron* 34: 255 – 264

Triller A, Choquet D (2008) New concepts in synaptic biology derived from single-molecule imaging. *Neuron* 59: 359 – 374

Vincent A, Irani SR, Lang B (2010) The growing recognition of immunotherapy-responsive seizure disorders with autoantibodies to specific neuronal proteins. *Curr Opin Neurol* 23: 144 – 150

Wang Z, Edwards JG, Riley N, Provance DW Jr, Karcher R, Li XD, Davison IG, Ikebe M, Mercer JA, Kauer JA, Ehlers MD (2008) Myosin Vb mobilizes recycling endosomes and AMPA receptors for postsynaptic plasticity. *Cell* 135: 535 – 548

Watt AJ, Sjostrom PJ, Hausser M, Nelson SB, Turrigiano GG (2004) A proportional but slower NMDA potentiation follows AMPA potentiation in LTP. *Nat Neurosci* 7: 518 – 524

Xiao MY, Karpefors M, Niu YP, Wigstrom H (1995) The complementary nature of long-term depression and potentiation revealed by dual component excitatory postsynaptic potentials in hippocampal slices from young rats. *Neuroscience* 68: 625 – 635

Xie X, Berger TW, Barrionuevo G (1992) Isolated NMDA receptor-mediated synaptic responses express both LTP and LTD. *J Neurophysiol* 67: 1009 – 1013

Yang J, Chamberlain SE, Woodhall GL, Jones RS (2008) Mobility of NMDA autoreceptors but not postsynaptic receptors at glutamate synapses in the rat entorhinal cortex. *J Physiol* 586(Pt 20): 4905 – 4924

Yashiro K, Philpot BD (2008) Regulation of NMDA receptor subunit expression and its implications for LTD, LTP, and metaplasticity. *Neuropharmacology* 55: 1081 – 1094

Yasuda H, Barth AL, Stellwagen D, Malenka RC (2003) A developmental switch in the signaling cascades for LTP induction. *Nat Neurosci* 6: 15–16

Zhang Q, Tanaka K, Sun P, Nakata M, Yamamoto R, Sakimura K, Matsui M, Kato N (2012) Suppression of synaptic plasticity by cerebrospinal fluid from anti-NMDA receptor encephalitis patients. *Neurobiol Dis* 45: 610–615

Zhu JJ, Esteban JA, Hayashi Y, Malinow R (2000) Postnatal synaptic potentiation: delivery of GluR4-containing AMPA receptors by spontaneous activity. *Nat Neurosci* 3: 1098–1106